Conventionally and SLM processed 18Ni300 steels: mechanical performance and tribological behaviour in dry sliding against PP40 composite

Daniel F. S. Ferreira [a, b, c*], G. Miranda [c, d], Filipe J. Oliveira [c, d], José M. Oliveira [a, b, c]

[a] EMaRT, Emerging Materials and Research Technologies, University of Aveiro, Portugal

[b] School of Design, Management and Production Technologies Northern Aveiro, Portugal

[c] CICECO, Aveiro Institute of Materials, University of Aveiro, Portugal

[d] Department of Materials and Ceramic Engineering, University of Aveiro, Portugal

---

Abstract

The high mechanical performance of 18Ni300 maraging steel, achieved during ageing treatment by precipitation of fine intermetallic precipitates within a martensitic matrix, makes this material a good choice for demanding applications such as injection moulds for the automotive industry. Its ease of manufacturing by selective laser melting (SLM) allows parts with a higher degree of complexity as well as the possibility of custom product design. Nevertheless, a comprehensive analysis of the performance of the manufactured parts is important to understand the differences between components manufactured by SLM and those produced by conventional methods.

In this work, the mechanical performance of a maraging steel 18Ni300 manufactured by SLM was compared with that of a commercial cast steel 18Ni300, as well as their tribological performance during dry sliding against a glass fibre polymer composite (PP40).

The results show that the steel as manufactured by SLM and aged at 510 ºC for six hours has higher hardness and better mechanical properties than the cast steel. Dry sliding wear tests of the aged steels against a polypropylene matrix composite reinforced with 40 wt% E-glass fibres showed a 33% lower specific wear rate for the steel manufactured by SLM compared to the cast steel. These results can be explained by the refined microstructure resulting from the rapid cooling during the SLM process. Different wear mechanisms were found: abrasion was the predominant mechanism for the steel manufactured by the SLM process, while abrasion and adhesion were observed for the cast steel.

Keywords: selective laser melting; casting; maraging steel; abrasion; adhesion; microstructure refinement.

---

* Corresponding author. E-mail address: dfferreira@ua.pt

1. Introduction

Powder bed fusion (PBF) technologies have gained a lot of attention in the context of industry 4.0, as they can be used to produce high-performance and customized complex parts, such as mould inserts with conformal cooling channels [1-3].

Selective laser melting (SLM) is a PBF process that uses a computer-controlled laser beam to melt thin layers of powders [4]. The process is always repeated by adding new layers of powders and melting the corresponding cross-section layer-by-layer until the part is fully formed. The unmelted powders can be reused in further components, which reduces material wastage [5]. The SLM process can be used to process various metal powders, such as 18Ni300 maraging steel, which has a very low carbon content [6]. This steel is currently used in aerospace and mould making, among other applications, and is a good candidate for SLM manufacturing due its good weldability, dimensional stability, and low residual stresses. This compares favourably with AISI H13 or D2 tool steels also used in the mould industry, but that are difficult to process by SLM due to their higher carbon content and different hardening mechanism.

The superior performance of maraging steels is achieved by the nanometric intermetallic compounds (e.g. Ni_3Mo, Ni_3Ti, FeMo, FeTi, etc.) that precipitate within the martensitic matrix during a thermal treatment, called ageing, at temperatures of about 500 ºC [6-8].

Unlike conventional casting processes, which are characterized by a typical cooling rate of about 10 to 70 K/s, SLM cooling is much faster (10^5 to 10^6 K/s), resulting in a particular refined microstructure very dissimilar to that of cast materials [9].

It is well known that microstructurally refined materials have better mechanical properties and wear behaviour [10]. These are important requirements for moulds as they have to withstand aggressive operating conditions e.g. when abrasive materials or certain pigments, such as TiO_2, are injected and when the parts are removed from the mould. In these cases, mould life is shortened, leading to higher costs, and increasing the rate of defective parts [11-16].

It has been reported that the improvement in mechanical properties of SLM manufactured materials is due to the refinement in grain size explained by the Hall-Petch effect as well as the high density of microstructural dislocations formed during the process [17,18]. This effect has been observed for various materials, such as 316L stainless steel [19,20], H11 steel [21], H13 steel [22] and Al- / Co-based alloys [23].

Over time, various studies have compared the performance of steels produced by different methods. It has been reported that 316L stainless steel manufactured by SLM process has a fine grain size (of about 10 µm), while the same steel obtained by casting has coarser grains (30 to 60 µm). These microstructural differences have been associated with the improved mechanical properties of SLM processed steel, such as yield stress (YS) and ultimate tensile strength (UTS) and lower ductility [24-27]. Bartolomeu et al. [28] and Zhu et al. [29] compared the microstructure of a SLM and a cast 316L stainless steel and reached the same conclusion, attributing the better mechanical properties and wear behaviour of the SLM manufactured steel to the refined microstructure. Similar results were reported by Rathod et al. [30] when

comparing the wear behaviour of an Al-12Si alloy manufactured by SLM and conventional casting [31].

Studies dealing with the wear behaviour of conventionally cast maraging steels 18Ni300 are rare. However, several studies have investigated the wear behaviour of SLM manufactured 18Ni300 maraging steel. Yin et al. [32] studied the wear behaviour of aged 18Ni300 manufactured by SLM in contact with WC and found that mainly adhesive wear occurs. Tan et al. [33] investigated the wear behaviour of aged 18Ni300 also manufactured by SLM in contact with a SiC counterface and reported that abrasion is the main wear mechanism.

Sun et al. [34] reported their results on high-speed sliding of 18Ni300 prepared by double vacuum melting against a 100Cr6 counterface and discovered two different wear mechanisms: adhesion at low load and oxidative wear at high load. A recent study by Vikhareva et al. [35] reported the wear performance of aged 18Ni300 manufactured by SLM in contact with a 22MnB5 steel under high temperature conditions. They found the same wear mechanisms at different temperatures, but with an increase in severity as temperature increased.

Bae et al. [36] used a ball-on-disc apparatus to evaluate the wear behaviour of a SLM manufactured 18Ni300 steel using balls of an AISI 52100 high carbon steel and ZrO_2 as counterface materials. They reported a dependence on the SLM build-up direction and found that the most promising build-up directions for better wear resistance are those that also lead to higher mechanical properties. These authors also reported that at lower loads (e.g., 5 N), the specific wear rate of horizontally manufactured specimens is significantly higher than that of specimens manufactured in the vertical direction. At higher loads (e.g., 50 N), the trend reverses, and the horizontally manufactured specimens have a lower specific wear rate than the vertically manufactured specimens.

The need for lightweight and high-performance materials for the automotive industry, has forced researchers to find new materials, namely glass fibre reinforced polymers produced by injection moulding [37,38]. The wear behaviour of polymers or polymer-based composites in sliding contacts with various steels is well reported in the literature [16, 39-44], however studies investigating the wear behaviour of steels in contact with these innovative glass fibre composite materials are hard to find. In one of the few studies, Hufenbach et al. [16] investigated the wear behaviour of a polypropylene loaded with 30 wt% type E glass fibres in contact with a commercially available 100Cr6 steel counterpart in a block-on-ring configuration.

To fill the existing research gap, a comparison of the mechanical properties and tribological behaviour in the dry sliding with a PP40 glass fibre composite, of a maraging steel 18Ni300 manufactured by SLM with an equivalent commercial cast steel is carried out in this work. A pin-on-disc apparatus was chosen to perform the dry sliding wear tests, as an approach to the wear conditions in the steel cavity of the moulds, despite not being a complete simulation of the tribological process under real conditions.

Microstructural differences were also highlighted to explain the final properties and main wear mechanisms when this steel, manufactured by SLM or by casting, is in dry sliding contact with PP40 composite.

2. Experimental procedure

2.1. Materials and specimens

Specimens of maraging steel 18Ni300 were manufactured by two different ways: using SLM process and by machining a commercially available cast plate, received in the solution-annealed condition (Böhler, Sweden).

For SLM manufacturing, a commercial powder of maraging steel 18Ni300 (Renishaw Ltd., UK) was used with spherical particles approximately following an unimodal Gaussian distribution with D_{50}=35 µm and D_{90}=48 µm. Scanning electron microscopy (SEM) images of the powder are shown in Figure 1 (a) and (b) and its chemical composition is summarized in Table 1.

The powder was processed into dense parts using an AM 500Q series SLM metal printing machine (Renishaw Ltd., UK) with four ytterbium lasers of 500 W and a spot of 80 µm. During the build process, a protective argon gas shield was circulated in a closed loop to prevent chemical reactions and avoid the formation of by-products in the build chamber. A stripe building strategy was used as it promotes homogeneous heat distribution, resulting in fewer defects and residual stresses in the parts, while maintaining a relatively high build rate [45]. After the deposition of each powder layer, the stripes were rotated clockwise 67º to achieve homogeneous heat distribution, with maximum variance achieved at 360º.

As this work was developed having in mind a practical application of the industrial partner of this study, the mould making company Simoldes Aços SA (Portugal), a set of extensively parameters optimized by the machine supplier was used in the SLM manufacturing to reduce the risk of warpage and defects: laser power 250 W, point distance 70 µm, exposure time 60 µs, hatch distance 75 µm and layer thickness 50 µm. Nevertheless, based on our previous work, this set of parameters was considered adequate to obtain dense parts with good microhardness and density [46].

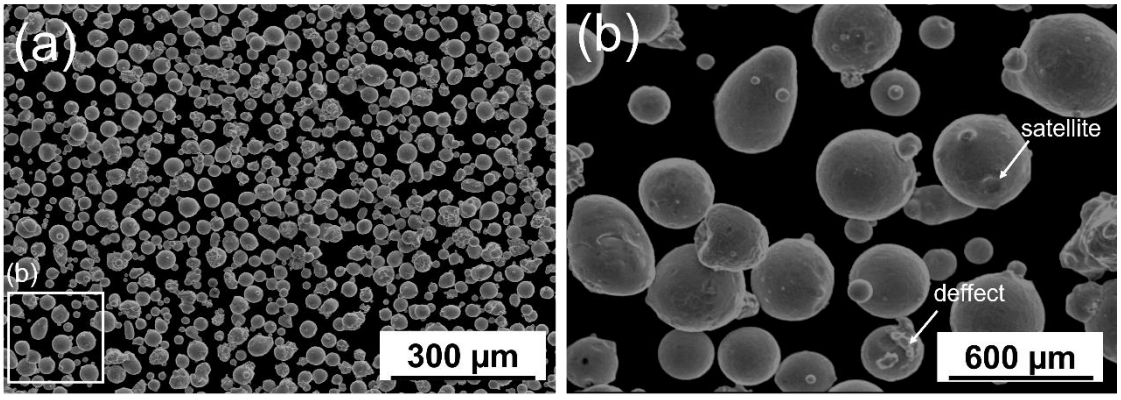

Figure 1- Maraging steel 18Ni300 for SLM: (a) low magnification and (b) high magnification.

Table 1- Chemical composition of maraging steel powder 18Ni300 analysed before SLM manufacturing (S.D. ±1 ppm).

Composition	Ni	Co	Mo	Ti	Si	Fe

wt%	17.58	8.86	5.25	0.50	0.37	Bal.

The second series of specimens was made from a conventionally cast maraging steel plate 18Ni300 with a length of 200 mm, a width of 50 mm and a thickness of 10 mm.

The samples obtained from both manufacturing routes were characterized mechanically in the as-built/as-received condition and after aging treatment, and their tribological properties were characterized only in the aged condition (the conditions of use of this steel).

The tensile specimens were prepared according to ASTM E8, while the specimens for the Charpy impact tests were prepared according to ASTM E23. Pins with two spherical tips and a diameter of 8 mm were obtained for the dry sliding wear tests. Steel discs with a diameter of 18 mm and a height of 10 mm were also used for microstructure characterization and microhardness measurements. The surface of the spherical pins and the top of the steel disc specimens were polished with 1 µm diamond paste. The ageing treatment in the samples was carried out at 510 ºC for six hours according to the procedure of Kučerová et al. [47].

The counterbody discs for performing the dry sliding wear tests were manufactured by injection moulding. The starting material was a commercial semi-crystalline thermoplastic polypropylene (PP) with 40 wt% short glass fibre type E (Borealis, Austria). Glass type E is known to have the following composition: silica (SiO_2) 52 to 54 wt%, alumina (Al_2O_3) 12 to 14 wt%, calcium oxide (CaO) 16 to 25 wt%, boron oxide (B_2O_3) 5 to 10 wt%, magnesia (MgO) <5 wt%, sodium oxide (Na_2O) <2 wt% and potassium oxide (K_2O) <2 wt% [48].

2.2. Phase identification and metallography

The crystalline phases of the prepared samples were identified with a Geigerflex X-ray diffractometer (Rigaku, Japan) using a Cu-Ka radiation source. The X-ray diffraction (XRD) spectra were recorded with a step size of 0.02º at 2θ angles from 20º to 100º.

For metallographic characterization, the polished sections of the metal disc samples (SLM and cast 18Ni300) were etched with Nital 15 vol% for 15 seconds and then examined using optical microscope (Nikon, Japan) and SEM (S4100, Hitachi, Japan).

2.3. Mechanical tests

Vickers indentation was performed with a pyramid tip on the polished top surface of the 18Ni300 steel discs, following ASTM E92-17. A durometer (Duramin, Struers, Denmark) was used, applying a constant load of 2 kgf for 15 seconds. Six indentations were measured to obtain a representative average value.

The tensile tests were performed in a universal testing machine (model AG-25TA from Shimadzu, Japan). The testing machine was not equipped with an extensometer and was used to accurately measure the actual applied load. The stress-strain curves were recorded with a crosshead displacement of 0.5 mm/s. The UTS was obtained directly from the results, while the

YS was determined graphically at 0.2% strain. To ensure reproducibility, three specimens were tested to determine the average stress values.

Charpy impact tests were also performed to measure the absorbed energy until the specimen fractured. The V-notched specimens were fractured using a vertical pendulum testing machine (Avery, UK) following the procedures of ASTM E 23-96. To ensure reproducibility, three samples were also tested to obtain an average value.

2.4. Dry sliding wear tests

Dry sliding wear tests were performed at room temperature (~23 ºC) and under ambient relative humidity conditions, using a rotating pin-on-disc apparatus in a tribometer model TE92 (Plint, UK). During the tests, spherical pins made of 18Ni300 maraging steel obtained by SLM and casting (after the ageing thermal treatment), were pressed against discs made of PP40 for 2000 seconds with a constant load of 40 N. The sliding speed was kept constant at 200 rpm with a sliding radius of 20 mm, corresponding to a linear velocity of 0.4 m/s (total distance of 800 m). The test conditions were chosen based on the literature review and our previous work that showed measurable and representative wear occurs under such conditions [43,44,49].

Three sets of samples were tested to ensure consistency of results. The coefficient of friction (COF) was constantly monitored by the machine and recorded for further analysis. Before and after each test, 3D optical profiles of the surface of the pins and PP40 discs were recorded using an optical profilometer model S-neox (Sensofar Metrology, Spain). The profiles obtained before and after the test were overlapped to determine the total worn volume on the surface of the pins and of the PP40 discs. The specific wear rate (k) was then calculated using Equation 1.

$$k = \frac{Worn\ volume\ (mm^3)}{Normal\ load\ (N) \times Sliding\ distance\ (m)} \quad (1)$$

After the test, the surfaces of the pins and discs were also observed using SEM and analysed chemically by energy dispersive x-ray spectroscopy (EDS). The wear debris resulting from the tests were carefully collected for SEM /EDS observation.

3. Results and discussion

3.1. Structural and microstructural analysis

Figure 2 shows the XRD patterns for the SLM and the cast 18Ni300, before and after ageing, respectively. Overall, the 18Ni300 manufactured by SLM (Figure 2 (a)) shows a martensitic microstructure with a small amount of retained austenite at 2θ values of 42.4º, 50.6º and 74.5º. Due to the micro segregation of certain elements at the cell boundaries (e.g. Ni), the austenite phase was stabilized as the initial temperature at which the martensite is converted to austenite decreases [42,43,50]. As the ageing treatment of the 18Ni300 manufactured by SLM process increases the amount of retained austenite, the peaks corresponding to martensite appear less intense [43].

The XRD pattern of the cast 18Ni300 before ageing (as-received condition) in Figure 2 (b), shows a fully martensitic structure without residual austenite. In the solution-annealed condition, the steel exhibits a lath-type martensitic structure typical of this class of steel, as explained in the work of Chakravarthi et al. [51]. After the ageing treatment, strong diffraction peaks at 44.6º and 64.9º also reveal a martensitic structure. A peak at 74.5º indicates that a residual amount of retained austenite is also present, which could be attributed to the reversion phenomenon. Xu et al. [52] stated that the austenite in the maraging steel 18Ni300 consists of retained austenite and reverted austenite. As for 18Ni300 manufactured by SLM, small diffraction peaks are also observed at 2θ values of 20.9º, 24.4º and 26.1º, which should correspond to intermetallic precipitates Ni_3(Al, Ti, Mo, Fe) formed during age hardening.

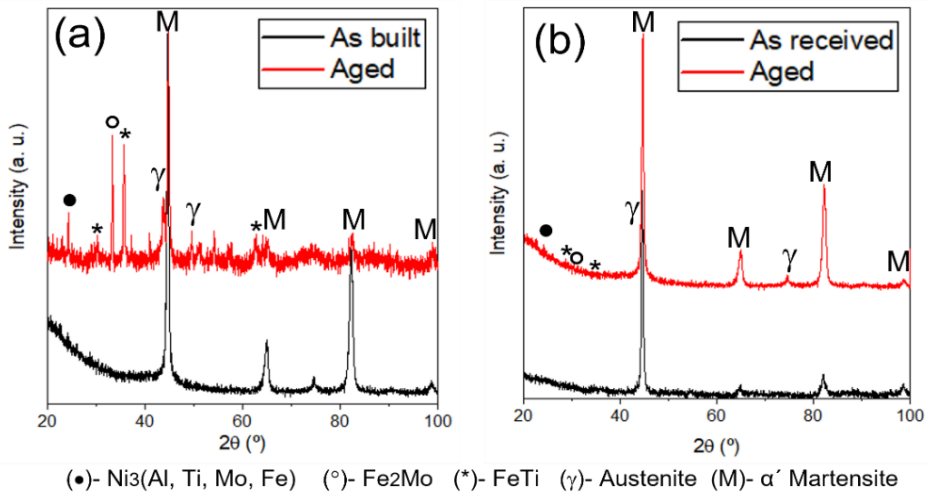

Figure 2- XRD pattern of maraging steel 18Ni300: (a) processed by SLM and (b) by conventional casting.

Figure 3 shows the micrographs of the polished and etched surfaces of the SLM manufactured and cast 18Ni300 before ageing treatment. In the horizontal cross-section of the SLM manufactured 18Ni300 (Figure 3 (a)), the laser marks with the respective 67º rotation angle are visible due to the scanning strategy used.

The cast 18Ni300 was also analysed in horizontal and vertical cross-sections (considering a hypothetical cuboid sample) to evaluate the microstructural differences. Figure 3 (b) shows the horizontal view in the as-received condition. A coarse lath-type martensitic structure can be seen, with no preferred orientations formed during the casting process.

In the vertical cross-section of the SLM manufactured 18Ni300 (Figure 3 (c)), individual melt pools can be seen, delineated by the corresponding melt pool boundary (MPB). The dimensions of the melt pool were determined using Image J software in the build direction and perpendicular to the build direction. They have a height of 46-70 µm and a width of 100-145 µm. Figure 3 (d) shows the vertical cross-section through the cast 18Ni300. As in the horizontal cross-section, a coarse lath-type microstructure with no preferred orientations can be seen, indicating that the material is quite isotropic.

In Figure 3 (e), a SEM magnification, taken between two representative melt pools of SLM manufactured 18Ni300, a fine cellular and dendritic structure can be seen. Interfaces

corresponding to MPBs are also visible. The MPB separates the dendritic from the fine cellular structure (in the middle of an adjacent melt pool). These dendrites are associated with the stronger thermal gradient in the MPB, while finer cells are present in the centre of the melt pool. Kučerová et al. [47] found a similar microstructure in maraging steel 18Ni300 manufactured by SLM.

The cast 18Ni300 was also analysed at higher magnification in SEM. Figure 3 (f) shows the SEM in as-received condition, and shows a homogeneous microstructure with no visible precipitates.

Overall, microstructural differences can be seen when comparing the SLM and cast microstructures of 18Ni300, also investigated by Król et al. [50]. These authors reported that the different thermal gradients and cooling rates are the driving force for the microstructural differences.

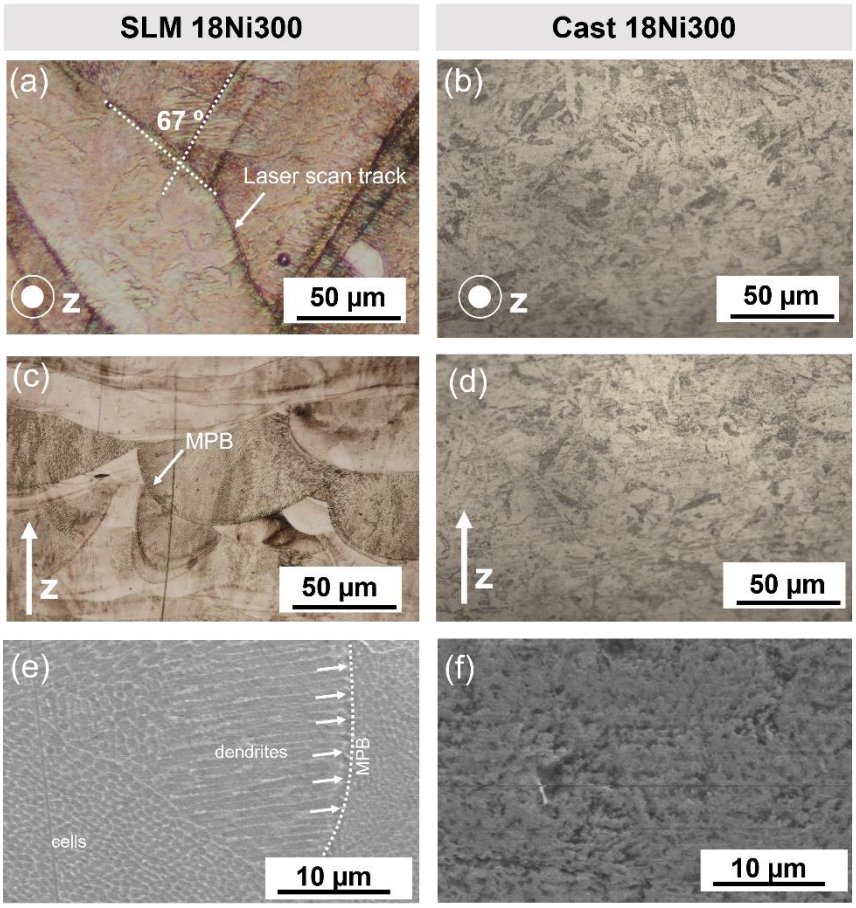

Figure 3- Cross-sectional images of 18Ni300 before ageing: (a) horizontal in SLM 18Ni300, (b) horizontal in cast 18Ni300, (c) vertical in SLM 18Ni300, (d) vertical in cast 18Ni300, (e) SEM observation of SLM 18Ni300 and (f) SM observation of cast 18Ni300.

Figure 4 shows SEM images of the polished and etched cross-sections of maraging steel 18Ni300 manufactured by SLM and casting after ageing. Overall, both microstructures are more homogeneous than before ageing. In the case of the 18Ni300 manufactured by SLM (Figure 4 (a) and (c)), the MPBs are less visible, and the cellular and dendritic structure (created by Ni segregation) has gradually disappeared (see the inset SEM image in the lower left corner of

Figure 4 (e)), creating nano-intermetallics within the martensitic structure (the typical hardening process) [50].

In the case of the cast 18Ni300 (Figure 4 (b) and (d)), the microstructure after ageing consists of martensite with the hardening phase dispersed in it (intermetallic). The high-magnification observation SEM in Figure 4 (f) shows a martensitic structure with lighter needles that should correspond to residual austenite. Although nanometric precipitates are present (see XRD pattern in Figure 2 (b)), they could not be detected by SEM due to their small size.

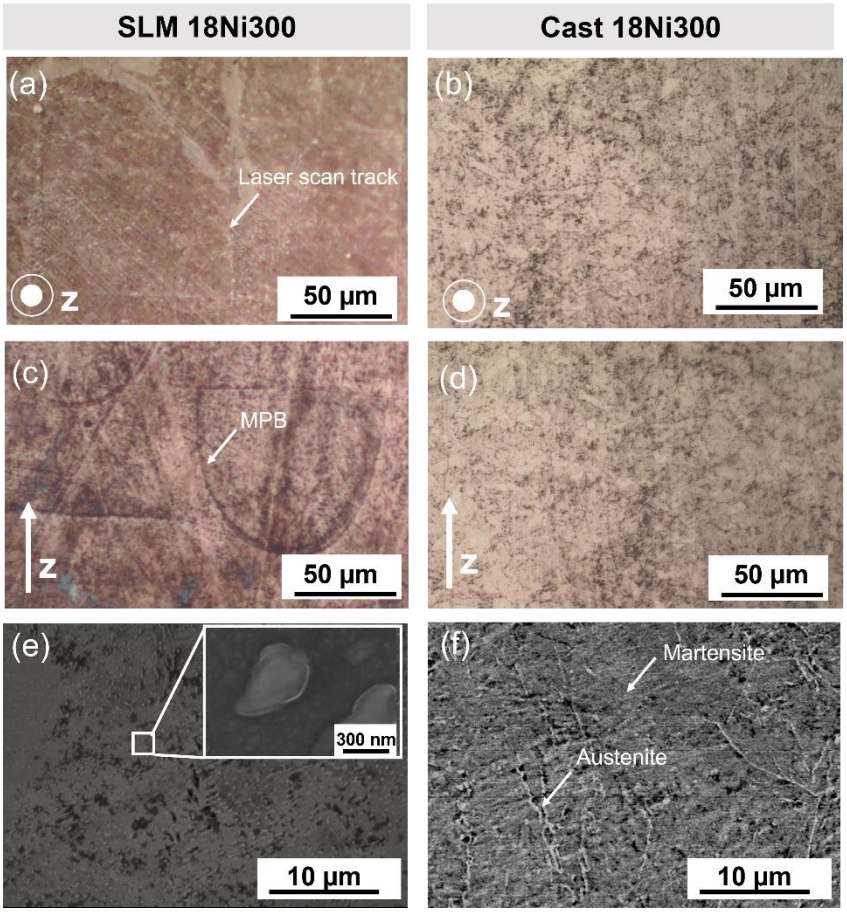

Figure 4- Cross-sectional images of 18Ni300 after ageing: (a) horizontal in SLM 18Ni300, (b) horizontal in cast 18Ni300, (c) vertical in SLM 18Ni300, (d) vertical in cast 18Ni300, (e) SEM observation of SLM 18Ni300 and (f) SEM observation of cast 18Ni300.

3.2. Mechanical characterization

The results of the tensile tests, microhardness evaluation and impact strength tests of the SLM manufactured and cast 18Ni300 before and after ageing are shown in the graphs in Figure 5 (a) and 5 (b). The stress-strain curves plotted during the tensile tests are also shown in Figure 6 and illustrate the changes in the behaviour of the steel due to the ageing treatment. The YS, UTS and microhardness for the "SLM as-built" are significantly higher than those for the "cast as-received" steel. These properties are larger by 16.0%, 23.8% and 17.6%, respectively.

Several authors reported similar results and attributed these higher mechanical properties to a refined microstructure as well as to the presence of intermetallic nanoprecipitates [53-57].

A significant increase of these properties was also observed after ageing the maraging steel 18Ni300 manufactured both by SLM (SLM aged) and by casting (cast aged), as can be seen clearly in Figure 5 (a). When comparing the mechanical properties before and after ageing, a high increase in hardness of 93% (cast) and 65% (SLM) was observed. At YS, ageing resulted in an increase of 101% (cast) and 83% (SLM). For UTS, the same trend was confirmed, with an increase of 94% (cast) and 68% (SLM) after ageing treatment. When comparing the SLM aged with the cast aged conditions, less pronounced increases were observed for the SLM processed steel with respect to the cast (aged) [58]: 5.4%, 7.5% and 7.5% for YS, UTS and the microhardness, respectively. This is due to the formation of intermetallic precipitates and consequent microstructural homogenization.

Charpy impact tests (Figure 5 (b)) show that the material exhibits more brittle behaviour after ageing: 1635 kJ/m^2 to 782 kJ/m^2 for the cast maraging steel 18Ni300 before and after ageing, respectively, and 1237 kJ/m^2 to 226 kJ/m^2 for the SLM manufactured maraging steel 18Ni300.

The stress-strain curves (Figure 6 (a) and (b)) also show that the plastic deformation was smaller after ageing treatment, indicating that the steel becomes more brittle due to the hardening process. The values obtained for the impact strength of the SLM manufactured maraging steel 18Ni300 are in the same order of magnitude as the values reported by Jarfors et al. [59]. These authors investigated the influence of different SLM scanning strategies (stripe, chessboard, and hexagon) on the impact strength and reported values between 147 kJ/m^2 and 555 kJ/m^2 for the aged steel.

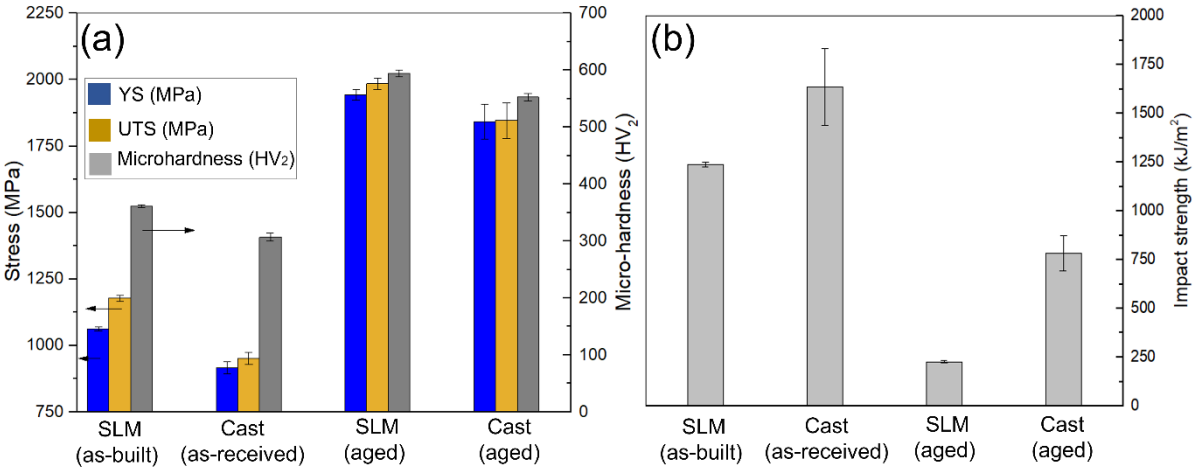

Figure 5- (a) Tensile properties and microhardness of SLM and cast 18Ni300, (b) Impact strength of SLM and cast 18Ni300.

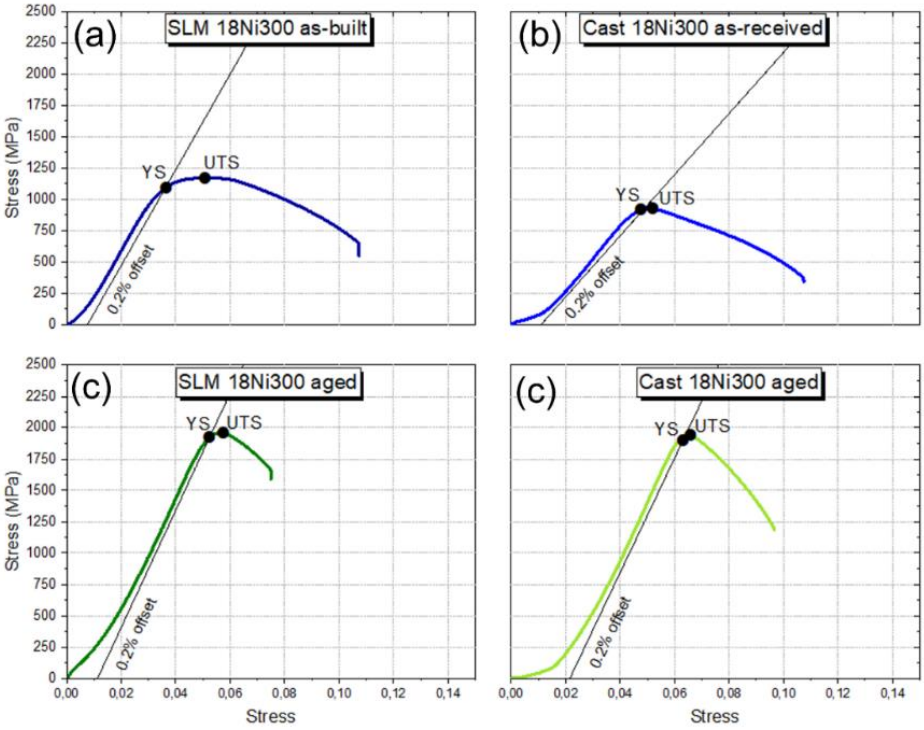

Figure 6- Representative stress-strain curves of the maraging steel 18Ni300 processed under different conditions. Note that no extensometer was used. (a) SLM manufactured 18Ni300 in as-built condition, (b) cast 18Ni300 in as-received condition, (c) SLM manufactured 18Ni300 aged and (d) cast 18Ni300 aged.

3.3. Dry sliding wear testing

The tribological tests were conducted using only the SLM and cast steel in their aged states, which is the condition of the steel when in real mould applications. Figure 7 shows representative COF curves recorded during the dry sliding wear tests with the different pairs: (a) SLM 18Ni300-PP40 and (b) cast 18Ni300-PP40. A similar COF evolution is observed for both pairs, starting with a run-in step and reaching average values of 0.3 to 0.4 after this. The COF values obtained are in line with those reported for general steel-polypropylene pairs [16, 60].

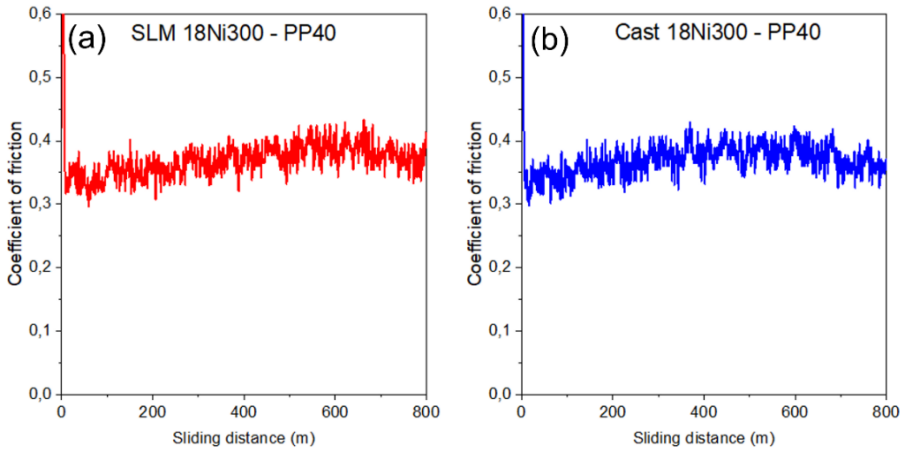

Figure 7- Coefficient of friction curves plotted during dry sliding wear tests: (a) SLM 18Ni300 -PP40 and (b) cast 18Ni300-PP40.

The resulting wear tracks in the PP40 disc were observed using optical profilometry. Figure 8 shows representative section profiles for each of the sliding pairs: (a) SLM 18Ni300-PP40 and (b) cast 18Ni300-PP40. After sliding against SLM 18Ni300, the PP40 showed a wear track with an approximate average depth and width of 30 µm and 1270 µm, respectively. On the PP40, after sliding against cast 18Ni300, wear tracks with a depth of 20 µm and a width of 1640 µm (average values) were observed. Knowing the depth, width and sliding radius, the worn volume and specific wear rate of the PP40 discs were calculated. The values are summarized in Table 2.

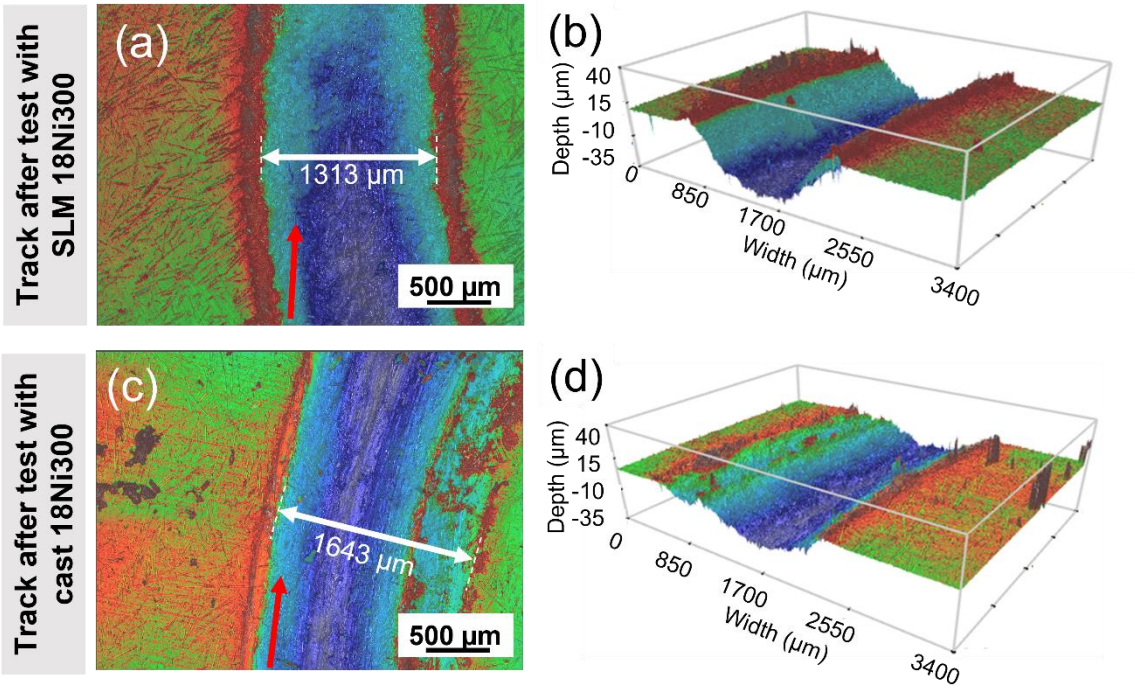

Figure 8- Representative profiles (2D and 3D) of the PP40 wear track after the dry sliding wear tests with: (a)-(b) SLM manufactured 18Ni300 and (c)-(d) cast 18Ni300. (*Note: Red arrows indicate the sliding direction*).

Table 2- Worn volume in maraging steel 18Ni300 and PP40 after tribological testing and corresponding specific wear rates. An average value with the standard deviation (S.D.) is given.

Sliding-pair	**Worn volume (mm^3)**				**Specific wear rate, k (mm^3/N.m)**			
	Steel pin ($\times10^{-2}$)		**PP40 (mm^3)**		**Steel pin ($\times10^{-6}$)**		**PP40**	
	Average	**S.D.**	**Average**	**S.D.**	**Average**	**S.D.**	**Average**	**S.D.**

SLM 18Ni300-PP40	6.59	0.69	3.96	0.09	1.84	0.22	1.24	0.03
Cast 18Ni300-PP40	8.77	0.23	1.83	0.15	2.74	0.07	0.57	0.05

The larger volume removed from the PP40 discs after sliding against SLM 18Ni300 pins (Table 2), results in a higher average specific wear rate of the polymer based composite when compared to cast 18Ni300 (k=1.24 and 0.57 mm^3/N.m, respectively). Figure 8 shows that deeper and wider wear tracks are formed on PP40 after sliding the maraging steel 18Ni300 manufactured by SLM.

The wear tracks on the PP40 discs formed during sliding with the pins were analysed using SEM/EDS. Iron was found in both wear tracks by EDS, suggesting some material transfer from both pins of maraging steel 18Ni300. The SEM images shown in Figure 9 (after sliding against (a) SLM and (b) cast 18Ni300) show evidence of softening of the polymer leading to plastic deformation. The frictional heat generated can lead to a temperature rise during sliding, softening the PP40.

The COF values (Figure 7) show that they slightly increase in the first 400 m of sliding, which could be related to the increasing temperature as the adhesion forces increase with the softening of the polymer. Several studies [44, 61] dealing with the tribological behaviour of steel-polymers suggest that an increase in COF may be the result of frictional heat when the frictional heat is directly proportional to the normal load and sliding velocity.

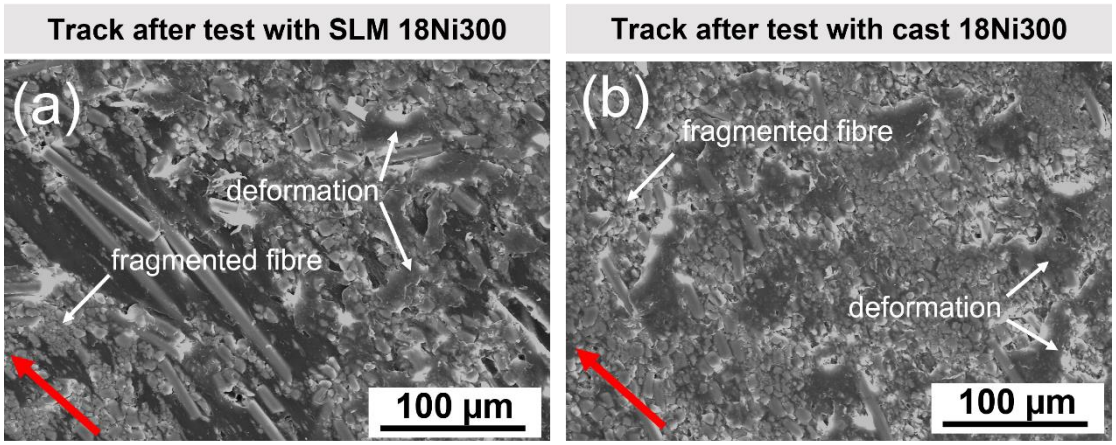

Figure 9- SEM images of the wear track of PP40 after dry sliding wear tests with: (a) SLM 18Ni300 and (b) cast 18Ni300 pins. (*Note: Red arrows indicate the sliding direction*).

The surfaces of the pins were analysed after each test to evaluate the morphological differences and to investigate the wear mechanisms that led to the rather different results in terms of worn volume and specific wear rate (see Table 2). The surfaces of the pins were examined before and after the test using 3D optical profilometry and SEM (Figure 10 and Figure 11, respectively). The 3D profiles, recorded by optical profilometry before and after the dry sliding tests, were overlapped to accurately determine the worn volume and calculate the

specific wear rate. As summarized in Table 2, the SLM manufactured 18Ni300 has a lower worn volume and specific wear rate ($k=1.84\times10^{-6}$ $mm^3/N.m$) compared to the cast material (2.74×10^{-6} mm^3/N). The higher mechanical properties (i.e., YS and UTS) and microhardness of the SLM manufactured 18Ni300 (Figure 5 (a)) led to the better wear performance of this material compared to the cast 18Ni300. The fine microstructure of SLM manufactured 18Ni300 (Figure 3 (e) and Figure 4 (e)), consisting of small cells and dendrites, is very different from that of the cast material in which coarse grains are present.

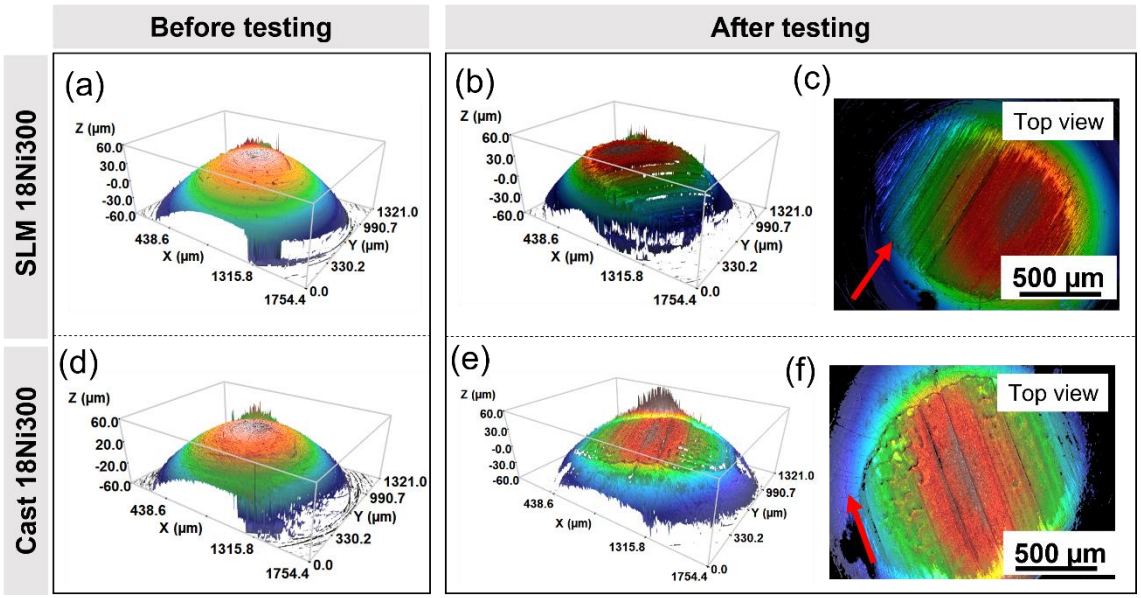

Figure 10- 3D surface profiles of the pins: (a) before dry sliding wear test with SLM manufactured 18Ni300 and (b)-(c) after dry sliding wear test with SLM manufactured 18Ni300, (d) before dry sliding wear test with cast 18Ni300 and (e)-(f) after dry sliding wear test with cast 18Ni300. (*Note: Red arrows indicate the sliding direction*).

After testing, coarse scratches are visible on the SLM manufactured 18Ni300 pins as seen in the micrographs o Figure 10 (c) and Figure 11 (a) and (b), indicating abrasive wear. The rotation of the pressed pin against the PP40 disc resulted in the tearing off of polypropylene and glass fibre fragments (hard asperities), which act as abrasive cutting bodies [62].

The analysis of the cast 18Ni300 pin, Figure 10 (f) and Figure 11 (c) and (d) showed signs of ploughing and plastic deformation. Due to the strong adhesion, the material was deformed and abraded, resulting in abrasion with subsequent formation of the so-called galling effect. This effect is usually observed due to high friction, poor lubrication or high contact pressure [63]. In this case, the more ductile behaviour of the cast 18Ni300 could have contributed to the plastic deformation during sliding. The mechanical properties (Figures 5 and 6) support this conclusion, as cast 18Ni300 exhibits a more ductile behaviour with lower microhardness and higher plasticity after ageing.

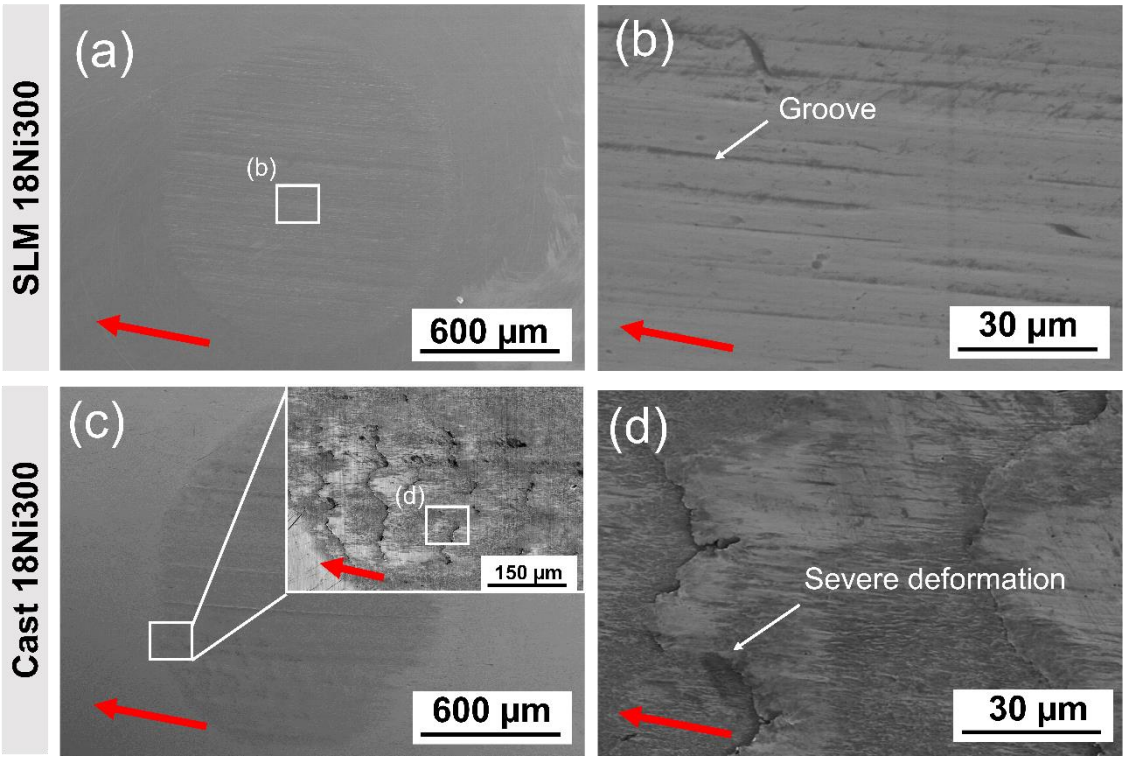

Figure 11- SEM images of the surfaces of the 18Nii300 pins after testing: (a)-(b) manufactured by SLM and (d)-(e) manufactured by casting. (*Note: Red arrows indicate the sliding direction*).

The wear debris produced during the dry sliding wear tests were examined using SEM (Figure 12). Their chemical composition was also analysed by EDS over the entire area shown in Figure 12 (a) and (c). In both cases, some irregular debris and roll-like fragments consisting of polypropylene, glass fibres, and iron were found, as shown by the spectrum of EDS (Figure 12 (a) and (c)). However, the iron peak is less intense when the SLM manufactured 18Ni300 was used. This could be due to the smaller amount of worn material in the SLM manufactured 18Ni300 pin compared to the casting (Table 2).

The roll-like shape of the debris was achieved by deforming the softened polypropylene fragments. This roll-like debris may act as a third rolling element and accelerate the wear of the two 18Ni300 pins [64, 65].

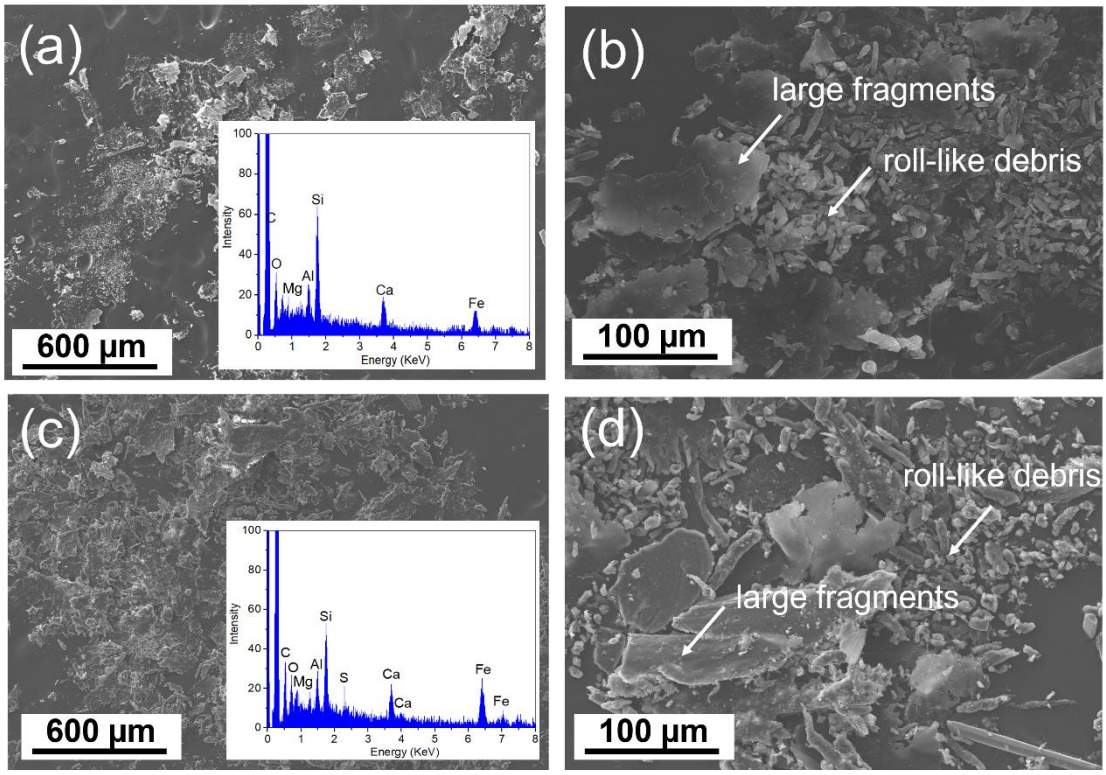

Figure 12- SEM observation and EDS chemical analysis of the resulting wear debris after testing with the different pairs: (a)-(b) SLM 18Ni300–PP40and (c)-(d) cast 18Ni300-PP40.

Conclusions

In this work, the mechanical properties and wear behaviour of a maraging steel 18Ni300 manufactured by SLM and casting were compared. The main conclusions are given below:

- The yield stress, ultimate tensile strength and microhardness were measured before and after ageing treatment, and for both conditions, the SLM manufactured 18Ni300 steel exhibited the highest values.
- The microstructure of maraging steel 18Ni300 has a direct influence on the mechanical properties and wear behaviour. The refined microstructure of the SLM manufactured steel due to rapid cooling leads to improved mechanical properties both before and after ageing, but at the expense of lower fracture toughness.
- The SLM manufactured 18Ni300 exhibited a 33% lower specific wear rate (1.84×10^{-6} $mm^3/N.m$) compared to the cast steel.
- Different wear mechanisms were observed: pure abrasion prevailed in the SLM manufactured 18Ni300, while abrasion with adhesion was observed in the cast material, which was attributed to the coarser microstructure and lower mechanical properties.
- Selective laser melting is a promising process for manufacturing high-performance and complex shapes, as it takes advantage of design freedom and microstructure refinement, resulting in parts with better mechanical properties and higher wear resistance.

Acknowledgements

A special acknowledgement to Simoldes Aços SA (Oliveira de Azeméis, Portugal) for the support and availability with the SLM machine for the steel sample's processing.

Formatting of funding sources

This work was developed within the scope of the project CICECO-Aveiro Institute of Materials, UIDB/50011/2020 & UIDP/50011/2020, financed by national funds through the FCT/MEC and co-financed by FEDER under the PT2020 Partnership Agreement, through POCI-01- 0247-FEDER-039842 (NanoSIM 3D).

References

[1] Mazur M, Leary M, McMillan M, Elambasseril J, Brandt M. SLM additive manufacture of H13 tool steel with conformal cooling and structural lattices. Rapid Prototyping Journal. 2016. doi:

[2] Kitayama S, Miyakawa H, Takano M, Aiba S. Multi-objective optimization of injection molding process parameters for short cycle time and warpage reduction using conformal cooling channel. The International Journal of Advanced Manufacturing Technology. 2017;88(5-8):1735-44. doi:10.1007/s00170-016-8904-x.

[3] Geenen K, Röttger A, Feld F, Theisen W. Microstructure, mechanical, and tribological properties of M3: 2 high-speed steel processed by selective laser melting, hot-isostatic pressing, and casting. Additive Manufacturing. 2019;28:585-99. doi: 10.1016/j.addma.2019.05.028.

[4] Yap CY, Chua CK, Dong ZL, Liu ZH, Zhang DQ, Loh LE, et al. Review of selective laser melting: Materials and applications. Applied physics reviews. 2015;2(4):041101. doi: 10.1063/1.4935926.

[5] Carluccio D, Bermingham M, Kent D, Demir AG, Previtali B, Dargusch MS. Comparative study of pure iron manufactured by selective laser melting, laser metal deposition, and casting processes. Advanced Engineering Materials. 2019;21(7):1900049. doi: 10.1002/adem.201900049.

[6] Bai Y, Yang Y, Xiao Z, Wang D. Selective laser melting of maraging steel: mechanical properties development and its application in mold. Rapid Prototyping Journal. 2018. doi:10.1108/RPJ-05-2017-0104.

[7] Jägle EA, Choi P-P, Van Humbeeck J, Raabe D. Precipitation and austenite reversion behavior of a maraging steel produced by selective laser melting. Journal of Materials Research. 2014;29(17):2072-9. doi:10.1557/jmr.2014.204.

[8] Turk C, Zunko H, Aumayr C, Leitner H, Kapp M. Advances in maraging steels for additive manufacturing. BHM Bergund Hüttenmännische Monatshefte. 2019;164(3):112-6. doi:10.1007/s00501-019-0835-z.

[9] Loh L-E, Chua C-K, Yeong W-Y, Song J, Mapar M, Sing S-L, et al. Numerical investigation and an effective modelling on the Selective Laser Melting (SLM) process with aluminium alloy

6061. International Journal of Heat and Mass Transfer. 2015;80:288-300. doi: 10.1016/j.ijheatmasstransfer.2014.09.014.
[10] Ralls AM, Kumar P, Menezes PL. Tribological Properties of Additive Manufactured Materials for Energy Applications: A Review. Processes. 2021;9(1):31. doi: 10.3390/pr9010031.
[11] Martínez-Mateo I, Carrión-Vilches F, Sanes J, Bermúdez M. Surface damage of mold steel and its influence on surface roughness of injection molded plastic parts. Wear. 2011;271(9-10):2512-6. doi: 10.1016/j.wear.2010.11.054.
[12] Van Acker K, Vercammen K. Abrasive wear by TiO2 particles on hard and on low friction coatings. Wear. 2004;256(3-4):353-61. doi: 10.1016/S0043-1648(03)00462-9.
[13] Bienk E, Mikkelsen N. Application of advanced surface treatment technologies in the modern plastics moulding industry. Wear. 1997;207(1-2):6-9. doi: 10.2474/trol.7.190.
[14] Valigi MC, Logozzo S, Affatato S. New challenges in tribology: Wear assessment using 3D optical scanners. Materials. 2017;10(5)U:548. doi: 10.3390/ma10050548.
[15] Pouzada A, Ferreira EC, Pontes A. Friction properties of moulding thermoplastics. Polymer Testing. 2006;25(8):1017-23. doi: 10.1016/j.polymertesting.2006.06.009.
[16] Hufenbach WA, Stelmakh A, Kunze K, Böhm R, Kupfer R. Tribo-mechanical properties of glass fibre reinforced polypropylene composites. Tribology international. 2012;49:8-16. doi: 10.1016/j.triboint.2011.12.010.
[17] Whang S-H. Nanostructured metals and alloys: processing, microstructure, mechanical properties and applications: Elsevier; 2011. doi:10.1016/b978-1-84569-670-2.50028-9.
[18] Gorsse S, Hutchinson C, Gouné M, Banerjee R. Additive manufacturing of metals: a brief review of the characteristic microstructures and properties of steels, Ti-6Al-4V and high-entropy alloys. Science and Technology of advanced MaTerialS. 2017;18(1):584-610. Doi: 10.1080/14686996.2017.1361305.
[19] Zhong Y, Liu L, Wikman S, Cui D, Shen Z. Intragranular cellular segregation network structure strengthening 316L stainless steel prepared by selective laser melting. Journal of Nuclear Materials. 2016;470:170-8. doi: 10.1016/j.jnucmat.2015.12.034.
[20] Prashanth K, Eckert J. Formation of metastable cellular microstructures in selective laser melted alloys. Journal of Alloys and Compounds. 2017;707:27-34. doi: 10.1016/j.jallcom.2016.12.209.
[21] Casati R, Coduri M, Lecis N, Andrianopoli C, Vedani M. Microstructure and mechanical behavior of hot-work tool steels processed by Selective Laser Melting. Materials Characterization. 2018;137:50-7. doi: 10.1016/j.matchar.2018.01.015.
[22] Mertens R, Vrancken B, Holmstock N, Kinds Y, Kruth J-P, Van Humbeeck J. Influence of powder bed preheating on microstructure and mechanical properties of H13 tool steel SLM parts. Physics Procedia. 2016;83:882-90. doi: 10.1016/j.phpro.2016.08.092.
[23] Prashanth K, Eckert J. Formation of metastable cellular microstructures in selective laser melted alloys. Journal of Alloys and Compounds. 2017;707:27-34. doi: 10.1016/j.jallcom.2016.12.209.

[24] Song B, Zhao X, Li S, Han C, Wei Q, Wen S, et al. Differences in microstructure and properties between selective laser melting and traditional manufacturing for fabrication of metal parts: A review. Frontiers of Mechanical Engineering. 2015;10(2):111-25. doi: 10.1007/s11465-015-0341-2.
[25] Herzog D, Seyda V, Wycisk E, Emmelmann C. Additive manufacturing of metals. Acta Materialia. 2016;117:371-92. doi: 10.1016/j.actamat.2016.07.019.
[26] Lewandowski JJ, Seifi M. Metal additive manufacturing: a review of mechanical properties. Annual review of materials research. 2016;46:151-86. doi: 10.1146/annurev-matsci-070115-032024.
[27] Barro Ó, Arias-González F, Lusquiños F, Comesaña R, del Val J, Riveiro A, et al. Effect of four manufacturing techniques (casting, laser directed energy deposition, milling and selective laser melting) on microstructural, mechanical and electrochemical properties of co-CR dental alloys, before and after PFM firing process. Metals. 2020;10(10):1291. doi: 10.3390/met10101291.
[28] Bartolomeu F, Buciumeanu M, Pinto E, Alves N, Carvalho O, Silva F, et al. 316L stainless steel mechanical and tribological behavior—A comparison between selective laser melting, hot pressing and conventional casting. Additive Manufacturing. 2017;16:81-9. doi:10.1016/j.addma.2017.05.007
[29] Zhu Y, Zou J, Chen X, Yang H. Tribology of selective laser melting processed parts: stainless steel 316 L under lubricated conditions. Wear. 2016;350:46-55. doi: 10.1016/j.wear.2016.01.004.
[30] Rathod HJ, Nagaraju T, Prashanth K, Ramamurty U. Tribological properties of selective laser melted Al12Si alloy. Tribology International. 2019;137:94-101. doi: 10.1016/j.triboint.2019.04.038.
[31] Yan X, Gao S, Chang C, Huang J, Khanlari K, Dong D, et al. Effect of building directions on the surface roughness, microstructure, and tribological properties of selective laser melted Inconel 625. Journal of Materials Processing Technology. 2021;288:116878. doi: 10.1016/j.jmatprotec.2020.116878.
[32] Yin S, Chen C, Yan X, Feng X, Jenkins R, O'Reilly P, et al. The influence of aging temperature and aging time on the mechanical and tribological properties of selective laser melted maraging 18Ni-300 steel. Additive Manufacturing. 2018;22:592-600. doi: 10.1016/j.addma.2018.06.005.
[33] Tan C, Zhou K, Kuang M, Ma W, Kuang T. Microstructural characterization and properties of selective laser melted maraging steel with different build directions. Science and technology of advanced materials. 2018;19(1):746-58. Doi: 10.1080/14686996.2018.1527645.
[34] Sun K, Peng W, Wei B, Yang L, Fang L. Friction and wear characteristics of 18Ni(300) maraging steel under high-speed dry sliding conditions. Materials. 2020;13(7):1485. doi: 10.3390/ma13071485.

[35] Vikhareva A, Macêdo G, Pelcastre L, Hardell J. High temperature tribological behaviour of additively manufactured tool material for applications in press hardening. Wear. 2021:203859. doi: 10.1016/j.wear.2021.203859.
[36] Bae K, Kim D, Lee W, Park Y. Wear Behavior of Conventionally and Directly Aged Maraging 18Ni-300 Steel Produced by Laser Powder Bed Fusion. Materials. 2021;14(10):2588. doi: 10.3390/ma14102588.
[37] Long A, Wilks C, Rudd C. Experimental characterisation of the consolidation of a commingled glass/polypropylene composite. Composites science and technology. 2001;61(11):1591-603. doi: 10.1016/S0266-3538(01)00059-8.
[38] Svensson N, Shishoo R, Gilchrist M. Manufacturing of thermoplastic composites from commingled yarns-A review. Journal of Thermoplastic Composite Materials. 1998;11(1):22-56. doi: 10.1177/089270579801100102.
[39] Yamaguchi Y. Tribology of plastic materials: their characteristics and applications to sliding components: Elsevier; 1990. doi:
[40] Hooke C, Kukureka S, Liao P, Rao M, Chen Y. The friction and wear of polymers in non-conformal contacts. Wear. 1996;200(1-2):83-94. doi: 10.1016/S0043-1648(96)07270-5.
[41] Lawrence C, Stolarski T. Rolling contact wear of polymers: a preliminary study. Wear. 1989;132(1):183-91. doi: 10.1016/0043-1648(89)90211-1.
[42] Zsidai L, Samyn P, Vercammen K, Van Acker K, Kozma M, Kalácska G, et al. Friction and thermal effects of engineering plastics sliding against steel and DLN-coated counterfaces. Tribology Letters. 2004;17(2):269-88. doi: 10.1023/b:tril.0000032453.09366.d4.
[43] Unal H, Mimaroglu A. Friction and wear behaviour of unfilled engineering thermoplastics. Materials & design. 2003;24(3):183-7. doi: 10.1016/S0261-3069(03)00018-9.
[44] Unal H, Sen U, Mimaroglu A. Dry sliding wear characteristics of some industrial polymers against steel counterface. Tribology International. 2004;37(9):727-32. doi: 10.1016/j.triboint.2004.03.002.
[45] Saunders M. Design for metal AM-a beginner's guide. Renishaw plc. 2021, Gloucestershire, UK.
[46] Ferreira DF, Miranda G, Oliveira FJ, Oliveira JM. Predictive models for an optimized fabrication of 18Ni300 maraging steel for moulding and tooling by Selective Laser Melting. Journal of Manufacturing Processes. 2021;70:46-54. doi: 10.1016/j.jmapro.2021.07.066.
[47] Kučerová L, Zetková I, Jandová A, Bystrianský M. Microstructural characterisation and in-situ straining of additive-manufactured X3NiCoMoTi 18-9-5 maraging steel. Materials Science and Engineering: A. 2019;750:70-80. doi: 10.1016/j.msea.2019.02.041.
[48] Cevahir A. Glass fibers. Fiber Technology for Fiber-Reinforced Composites: Elsevier; 2017. p. 99-121. doi: 10.1016/B978-0-08-101871-2.00005-9.
[49] Ferreira DF, Vieira JS, Rodrigues S, Miranda G, Oliveira FJ, Oliveira JM. Dry sliding wear and mechanical behaviour of selective laser melting processed 18Ni300 and H13 steels for moulds. Wear. 2022;488:204179. Doi: 10.1016/j.wear.2021.204179.

[50] Król M, Snopiński P, Czech A. The phase transitions in selective laser-melted 18-NI (300-grade) maraging steel. Journal of Thermal Analysis and Calorimetry. 2020:1-8. doi: 10.1007/s10973-020-09316-4.
[51] Chakravarthi K, Koundinya N, Murty SN, Rao BN. Microstructural evolution and constitutive relationship of M350 grade maraging steel during hot deformation. Journal of Materials Engineering and Performance. 2017;26(3):1174-85. doi: 10.1007/s11665-017-2539-4.
[52] Xu X, Ganguly S, Ding J, Guo S, Williams S, Martina F. Microstructural evolution and mechanical properties of maraging steel produced by wire + arc additive manufacture process. Materials Characterization. 2018;143:152-62. doi: 10.1016/j.matchar.2017.12.002.
[53] Carluccio D, Bermingham M, Kent D, Demir AG, Previtali B, Dargusch MS. Comparative study of pure iron manufactured by selective laser melting, laser metal deposition, and casting processes. Advanced Engineering Materials. 2019;21(7):1900049. doi:10.1002/adem.201900049.
[54] Sander J, Hufenbach J, Giebeler L, Wendrock H, Kühn U, Eckert J. Microstructure and properties of FeCrMoVC tool steel produced by selective laser melting. Materials & Design. 2016;89:335-41. doi: 10.1016/j.matdes.2015.09.148.
[55] Kang N, Coddet P, Chen C, Wang Y, Liao H, Coddet C. Microstructure and wear behavior of in-situ hypereutectic Al–high Si alloys produced by selective laser melting. Materials & Design. 2016;99:120-6. doi: 10.1016/j.matdes.2016.03.053.
[56] Gu D, Hagedorn Y-C, Meiners W, Wissenbach K, Poprawe R. Nanocrystalline TiC reinforced Ti matrix bulk-form nanocomposites by Selective Laser Melting (SLM): Densification, growth mechanism and wear behavior. Composites Science and Technology. 2011;71(13):1612-20. doi: 10.1016/j.phpro.2014.08.153.
[57] Kumar S, Kruth JP. Wear performance of SLS/SLM materials. Advanced Engineering Materials. 2008;10(8):750-3. doi: 10.1002/adem.200800075.
[58] Tan C, Zhou K, Ma W, Zhang P, Liu M, Kuang T. Microstructural evolution, nanoprecipitation behavior and mechanical properties of selective laser melted high-performance grade 300 maraging steel. Materials & Design. 2017;134:23-34. doi: 10.1016/j.matdes.2017.08.026.
[59] Jarfors AE, Shashidhar ACGH, Yepur HK, Steggo J, Andersson N-E, Stolt R. Build Strategy and Impact Strength of SLM Produced Maraging Steel (1.2709). Metals. 2021;11(1):51. doi: 10.3390/met11010051.
[60] Korpela TE, Salstela J, Suvanto M, Pakkanen TT. Periodically micro-patterned viscose fiber-reinforced polypropylene composites with low surface friction. Wear. 2014;310(1-2):20-6. doi: doi.org/10.1016/j.wear.2013.12.003.
[61] Mens J, De Gee A. Friction and wear behaviour of 18 polymers in contact with steel in environments of air and water. Wear. 1991;149(1-2):255-68. doi: 10.1016/0043-1648(91)90378-8.
[62] Stachowiak G, Batchelor AW. Engineering tribology: Butterworth-Heinemann; 2013. ISBN: 978-0-12-397047-3.

[63] Kakulite KK, Panwar SS, Kandasubramanian B. A review: advancements in fluoro-based polymers for aggrandizing anti-galling and wear resistant characteristics. SN Applied Sciences. 2019;1(8):1-24. doi: 10.1007/s42452-019-0924-3.
[64] Mouritz A. Polymers for aerospace structures. Introduction to Aerospace Materials. 2012:268-302. doi: 10.1533/9780857095152.268.
[65] Pieniak D, Gauda K. Indentation Hardness and Tribological Wear under the Conditions of Sliding Friction of the Surface Layer of Composites Based on Methacrylate Resins with Ceramic Nanofiller. Advances in Science and Technology Research Journal. 2020;14:2. doi: 10.12913/22998624/118867.

FIG_1

Click here to access/download;Figure;FIG_1.tif

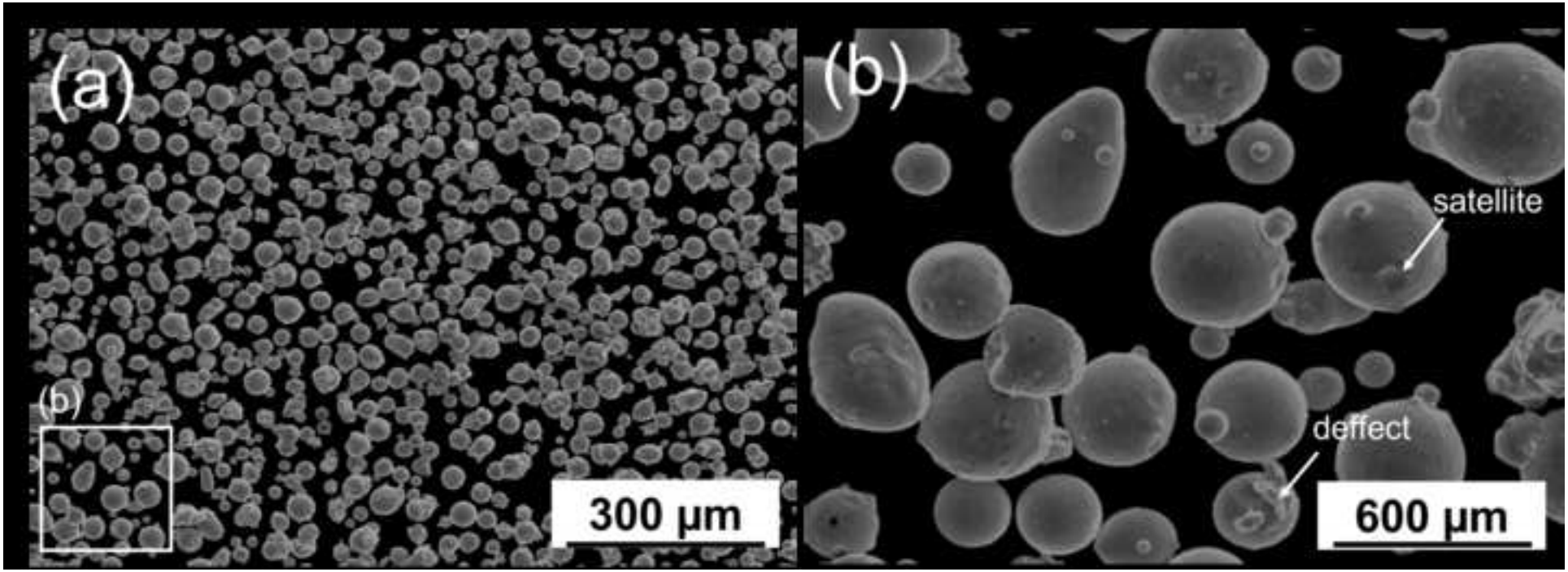

FIG_2

Click here to access/download;Figure;FIG_2.tif

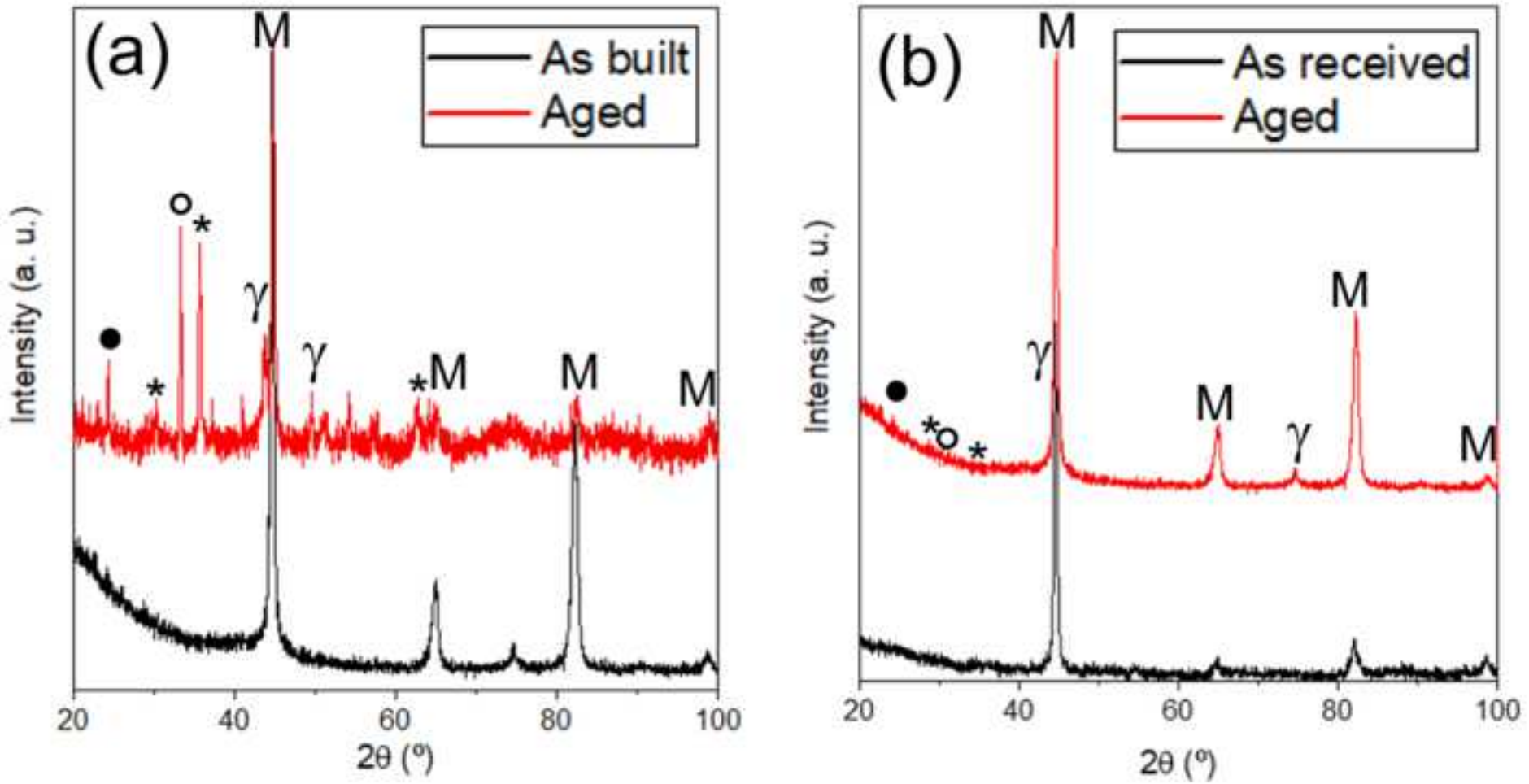

(•)- Ni3(Al, Ti, Mo, Fe) (°)- Fe2Mo (*)- FeTi (γ)- Austenite (M)- α´ Martensite

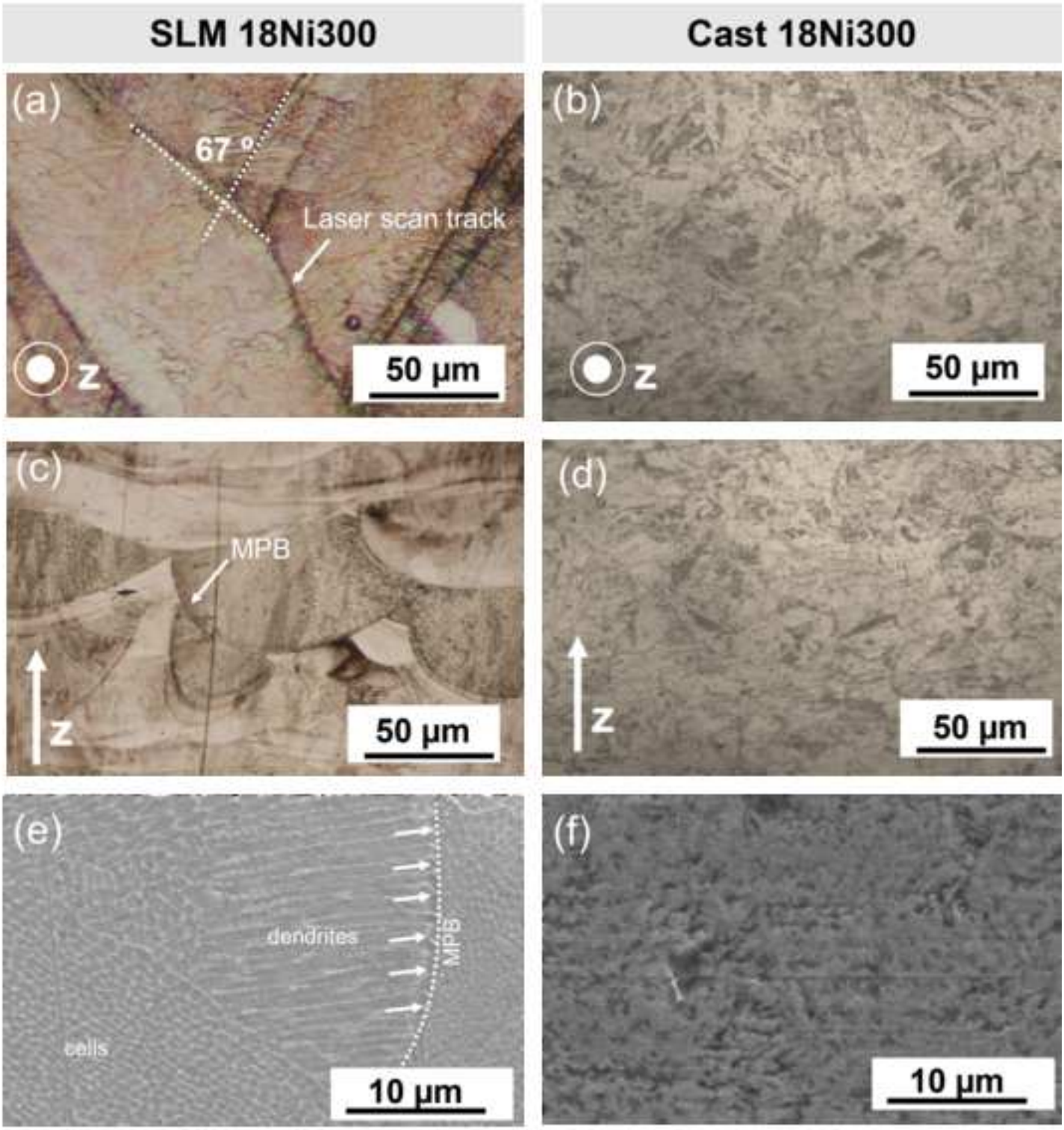

FIG_4

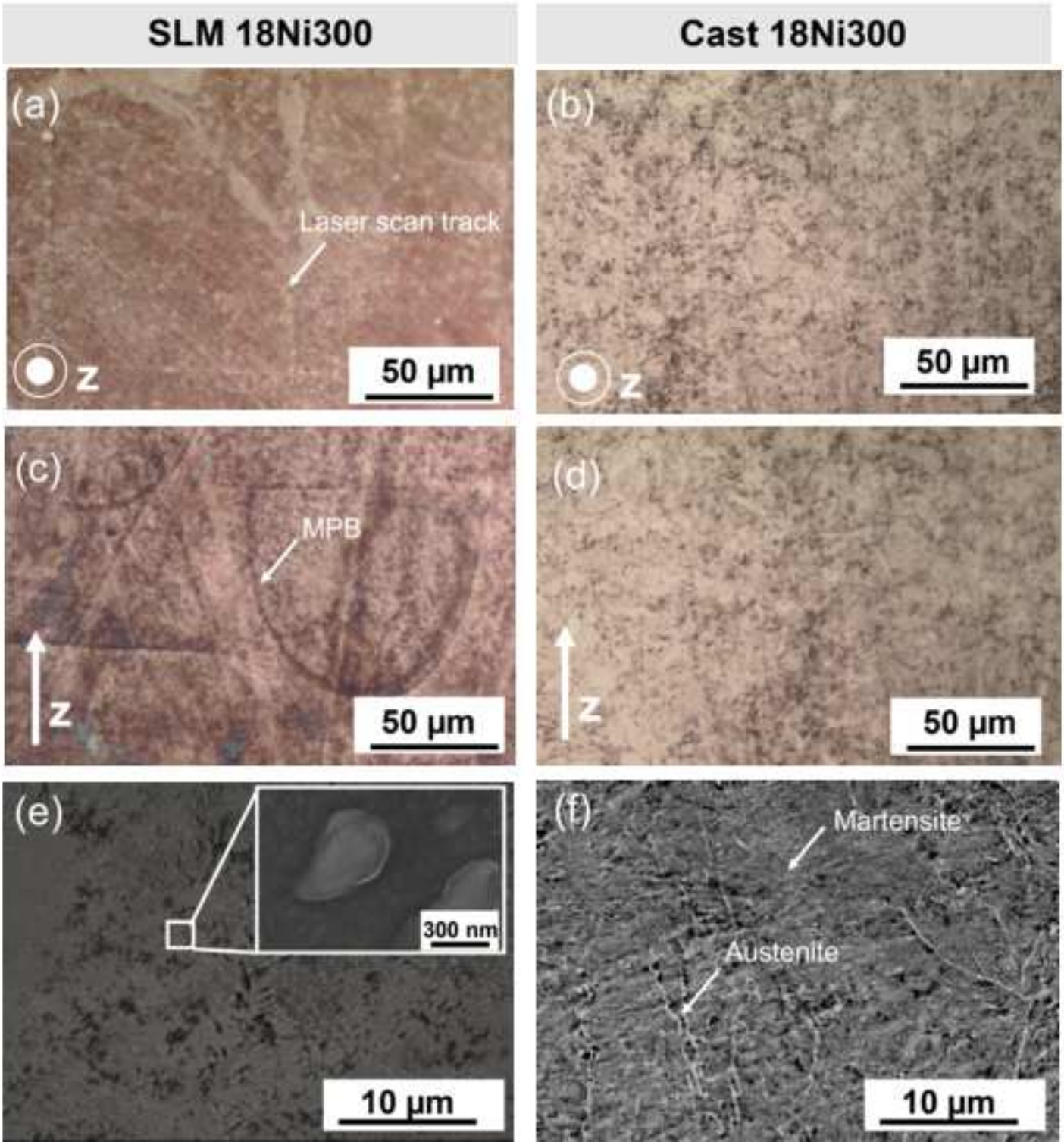

FIG_5

Click here to access/download;Figure;FIG_5.tif

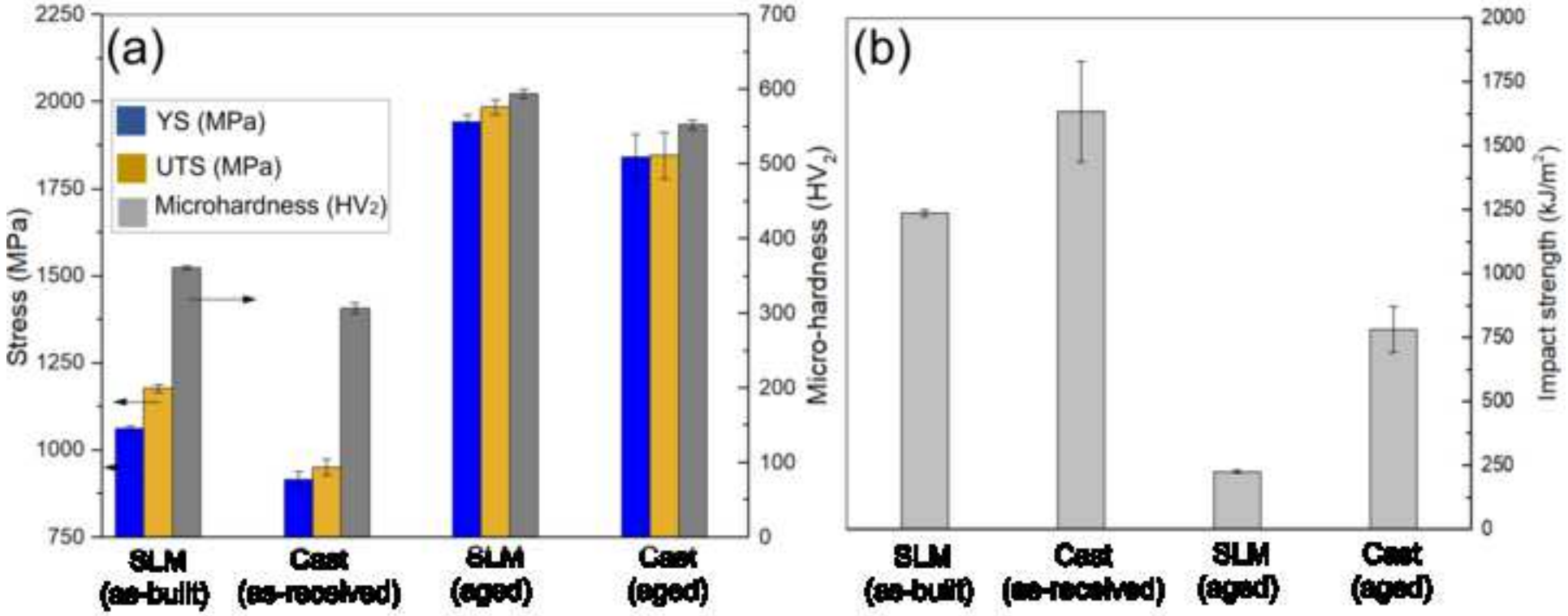

FIG_6

Click here to access/download;Figure;FIG_6.tif

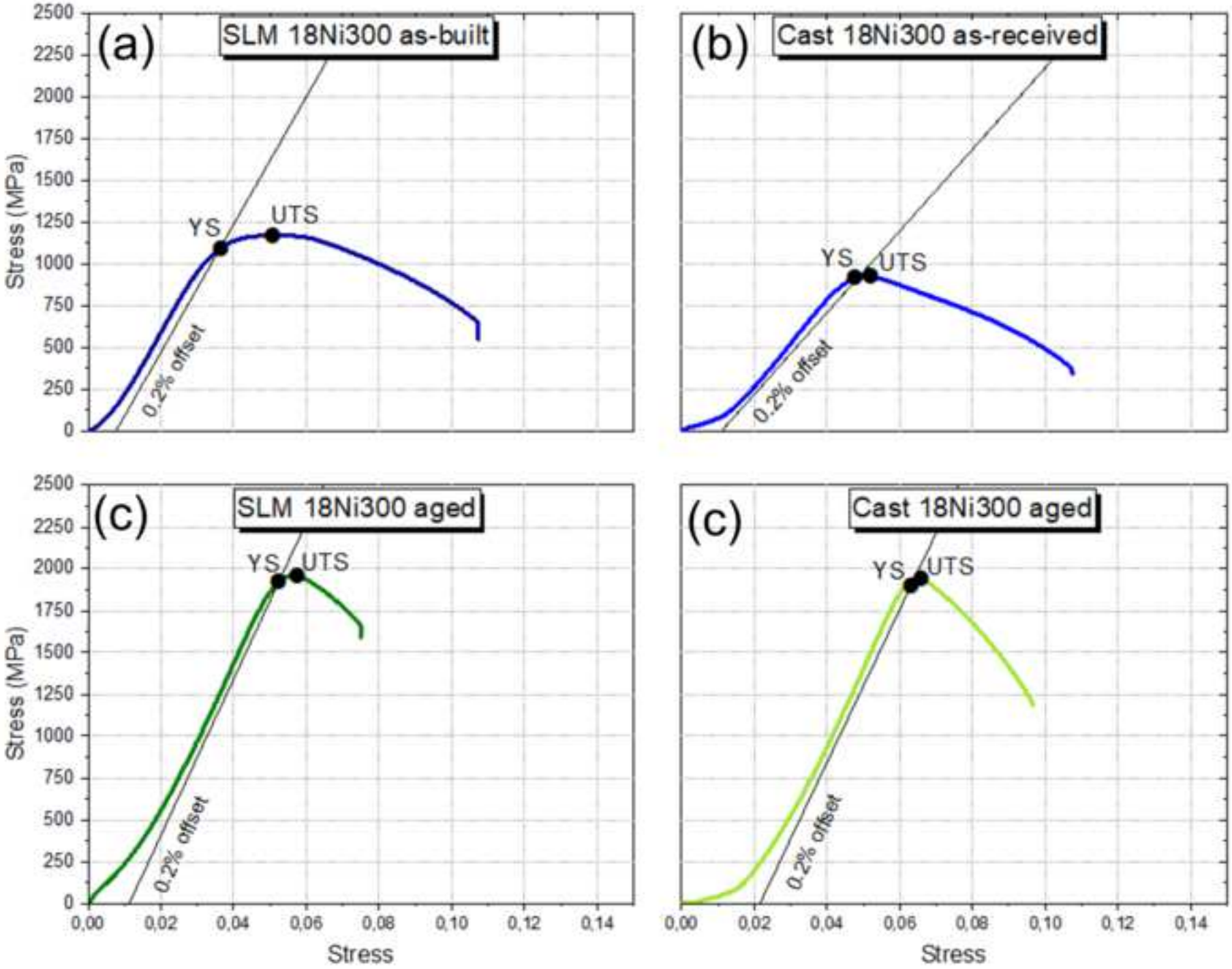

FIG_7

Click here to access/download;Figure;FIG_7.tif

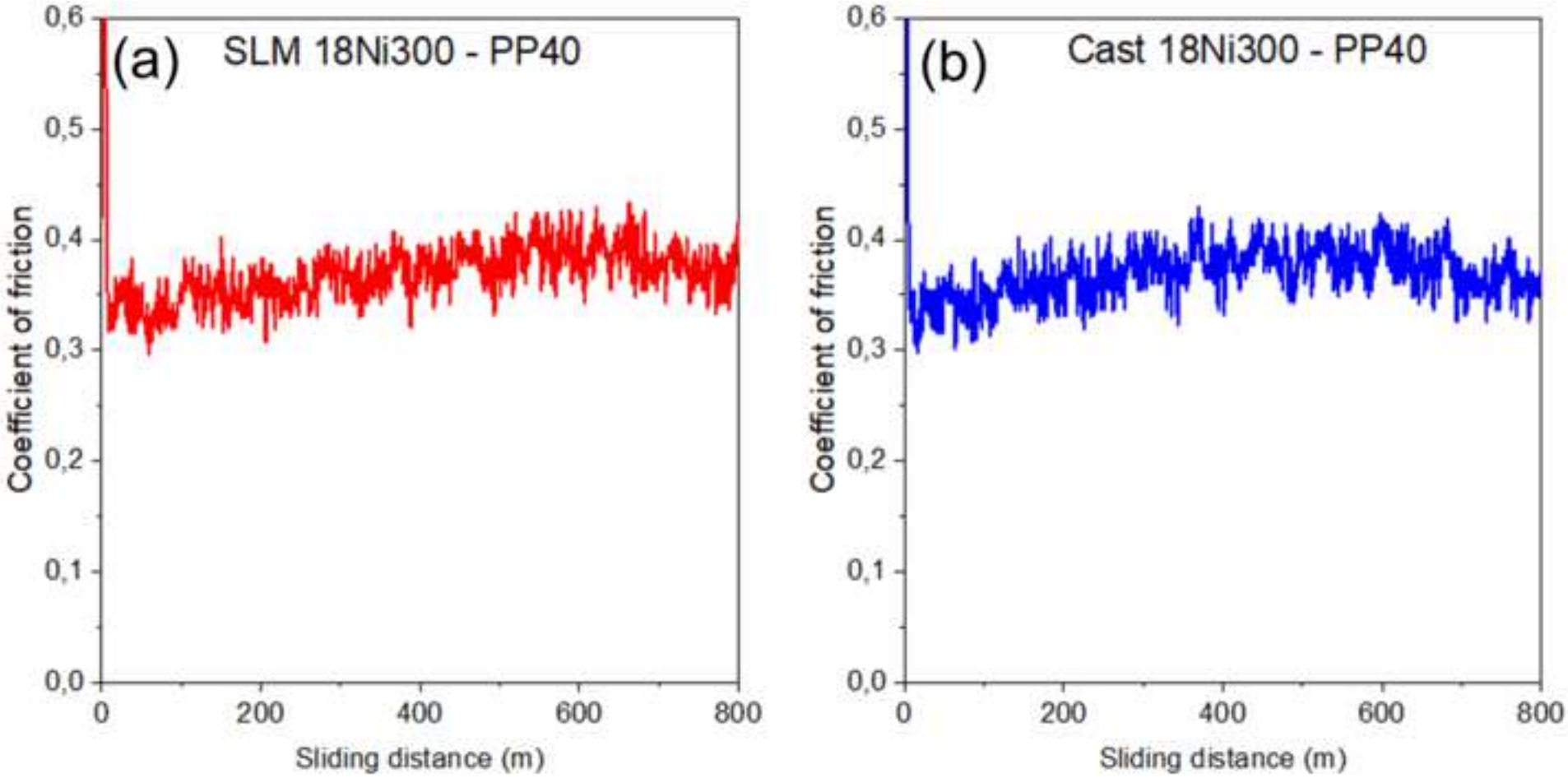

FIG_8

Click here to access/download;Figure;FIG_8.tif

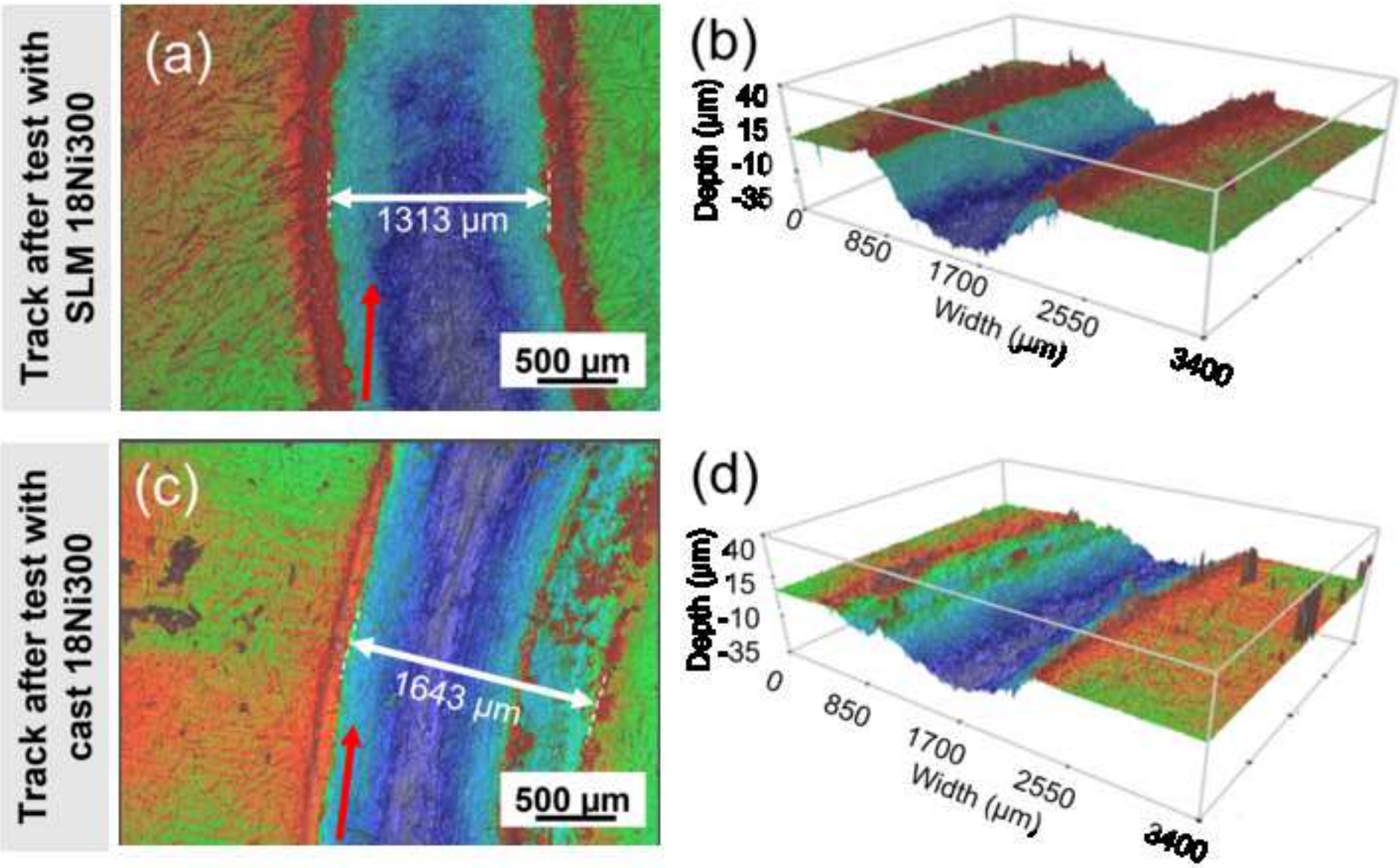

FIG_9

Click here to access/download;Figure;FIG_9.tif

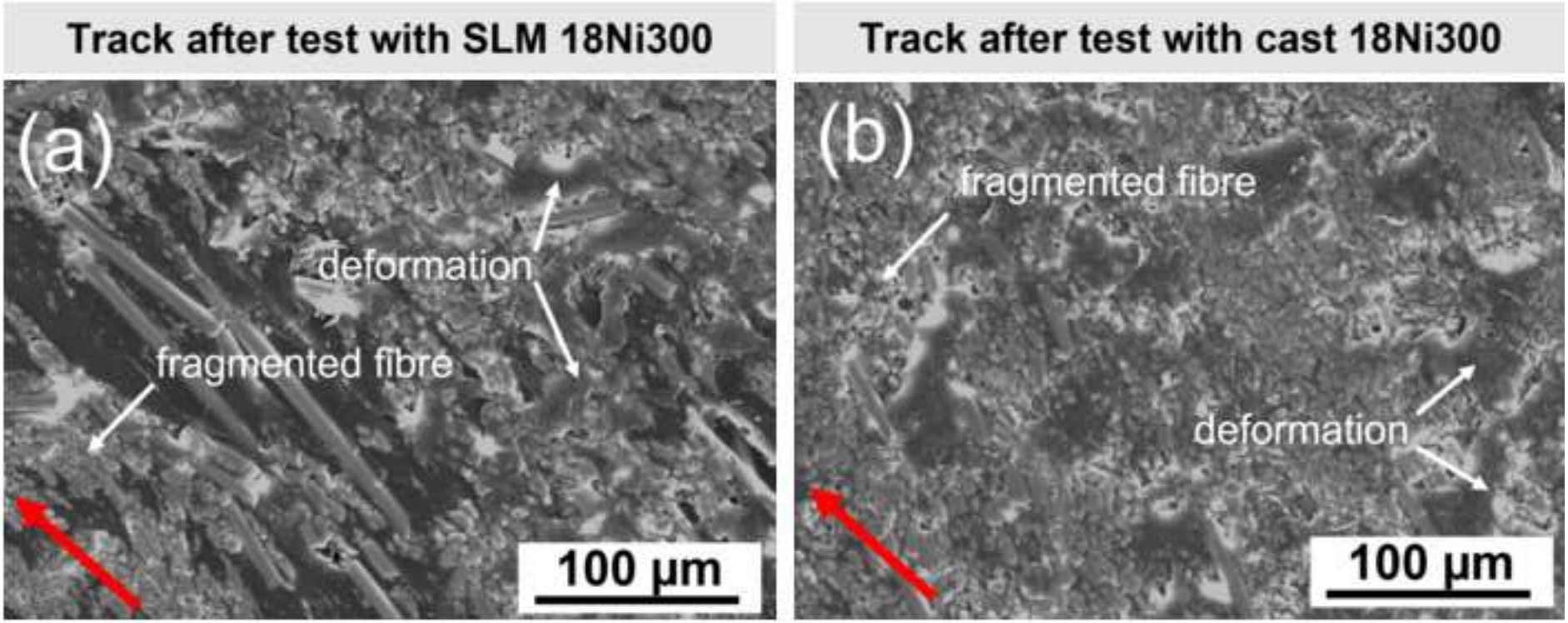

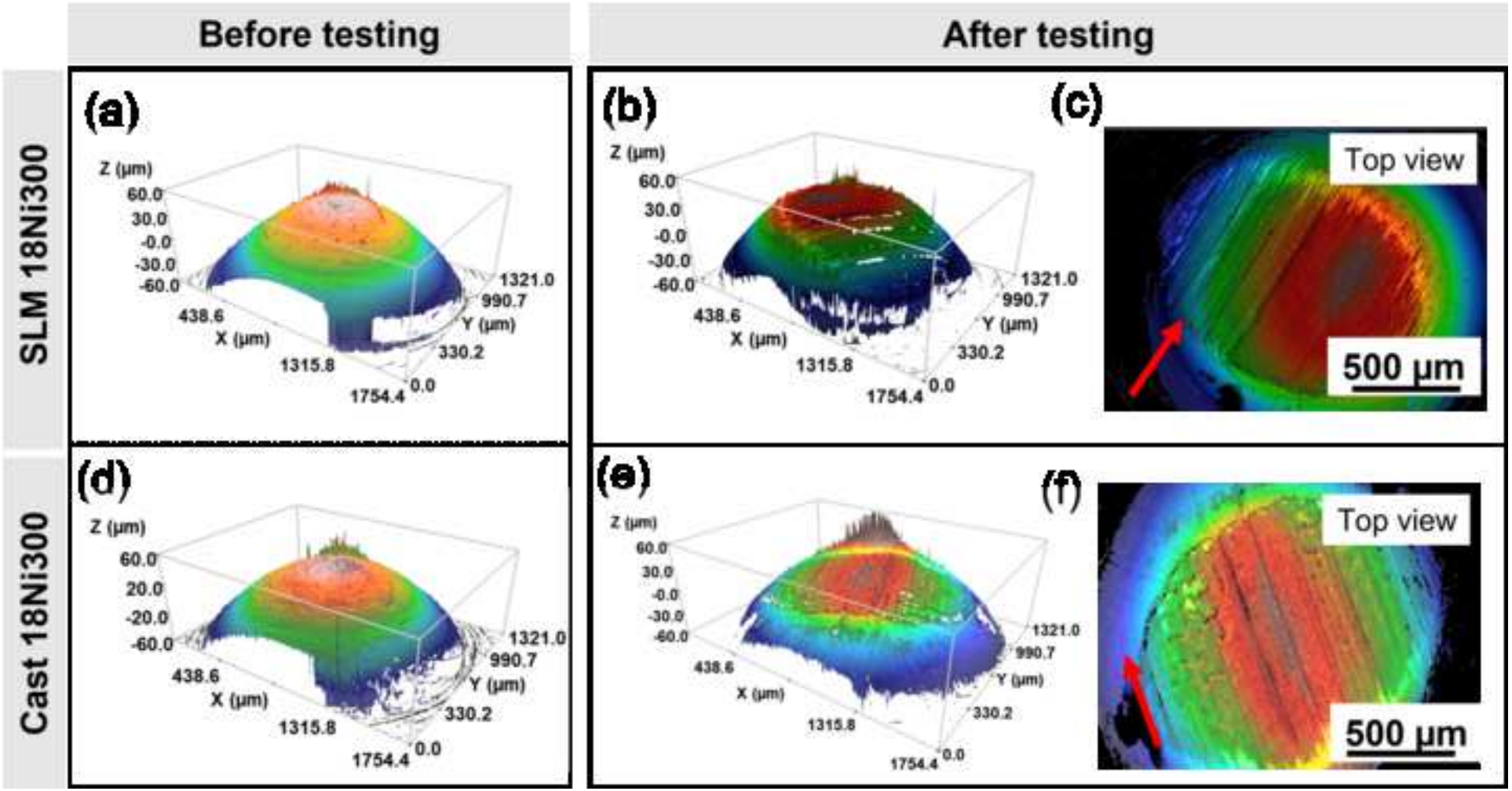

FIG_11

Click here to access/download;Figure;FIG_11.tif

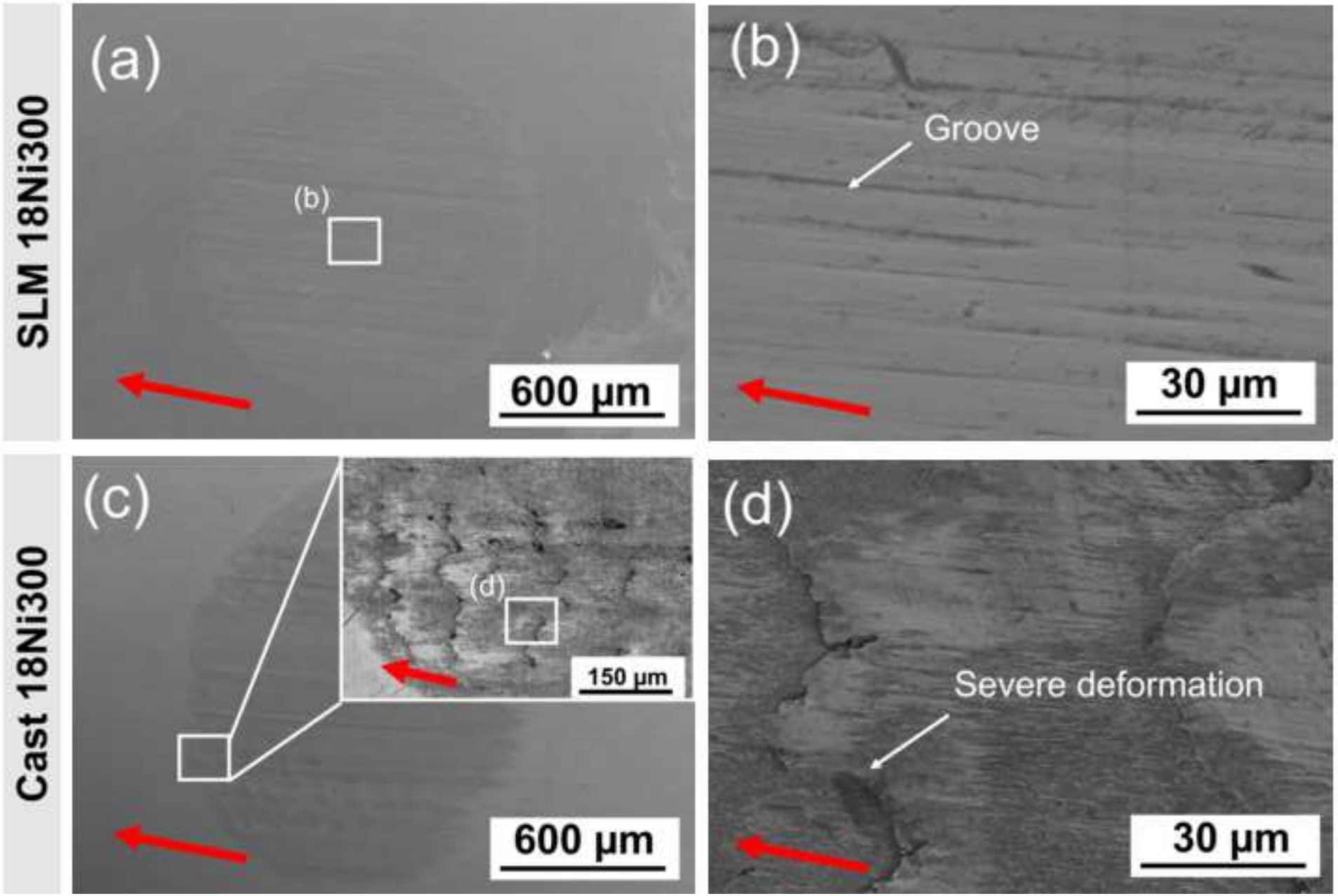

FIG_12

Click here to access/download;Figure;FIG_12.tif